

## Supplementary information

### S 1. Description of the LTE fits of the detected molecules toward the G31.41 shock position

In the following subsections, we describe the LTE fits of all the detected molecules in the G31.41 shock region, whose results are summarized in Table B.1. The transitions used for each molecule are listed in Table S 1, and they are plotted in Figs. 2, 3 and 4, and in the Appendix S 3.

#### S 1.1. Deuterated Ammonia ( $\text{NH}_2\text{D}$ )

Two transitions of  $\text{NH}_2\text{D}$ ,  $1_{1,1,0} \rightarrow 1_{0,1,1}$  and  $1_{1,1,1} \rightarrow 1_{0,1,0}$  are detected (see Fig. S 1). In this case, we add a second component to reproduce the line profile, and we fit the temperature value of each component to 20 K (see Table B.1), as explained in Sect. 3.2.1. The transitions are optically thin in both components ( $\tau < 0.088$ , see Table S 1). We derive values of the column densities for the two components of  $7.5$  and  $2.2 \times 10^{13} \text{ cm}^{-2}$ .

#### S 1.2. Ethynyl ( $\text{CCH}$ )

The hyperfine transitions of the  $1 \rightarrow 0$  rotational transition are clearly detected, and they appear unblended, as shown in Fig. S 2. The transitions are optically thin, covering a range of  $\tau$  from 0.08 to 0.4 (see Table S 1). Despite all the transitions sharing the same  $E_{\text{up}}$  of 4.2 K (Table S 1), the different line opacities allow to constrain the excitation temperature to  $13 \pm 7$  K. The derived column density is  $9.2 \times 10^{14} \text{ cm}^{-2}$ .

#### S 1.3. Hydrogen cyanide ( $\text{HCN}$ )

The  $\text{HCN } 1 \rightarrow 0$  transition appears in absorption, which can be due to filtering of extended emission by the interferometer and/or possible infall motions (see Fig. S 3). This prevents us to perform a proper fit. Therefore, we estimated its column density using one of their isotopologs.  $\text{H}^{13}\text{CN}$  is optically thicker than  $\text{HC}^{15}\text{N}$  ( $\tau = 0.13$  and  $0.056$  respectively; see Table S 1). Therefore, we use  $\text{HC}^{15}\text{N}$  molecule to obtain the fit of  $\text{HCN}$ . Fitting its temperature to 20 K, and using the  $^{14}\text{N}/^{15}\text{N}$  isotopic ratio, we obtained a final  $\text{HCN}$  column density of  $4.4 \times 10^{15} \text{ cm}^{-2}$  (see Table B.1).

#### S 1.4. Hydrogen cyanide ( $\text{HNC}$ )

Similarly to  $\text{HCN}$ , the  $\text{HNC } 1 \rightarrow 0$  transition shows an absorption profile probably due to filtering of extended emission and/or infall, which prevents us to perform the fit (see Fig. S 4). The  $1-0$  transitions of the  $\text{HN}^{13}\text{C}$  and  $\text{H}^{15}\text{NC}$  isotopologs are detected and appear unblended (see Fig. S 4). Since the  $\text{H}^{15}\text{NC}$  line is very weak and close to the noise of the spectrum, we have chosen  $\text{HN}^{13}\text{C}$  to obtain the  $\text{HNC}$  column density. We derived a value of  $4.9 \times 10^{14} \text{ cm}^{-2}$  by applying the  $^{12}\text{C}/^{13}\text{C}$  isotopic ratio (see Table B.1).

#### S 1.5. Carbon monoxide ( $\text{CO}$ )

The  $1 \rightarrow 0$  transitions of  $\text{CO}$  and  $^{13}\text{CO}$  also show line profiles severely affected by absorption (see Fig. S 5), so we have not performed their fits. The remaining detected isotopologs ( $\text{C}^{18}\text{O}$ ,  $\text{C}^{17}\text{O}$  and  $^{13}\text{C}^{18}\text{O}$ ) are significantly less affected by the absorption, and hence we performed the LTE fits. We used the optically thinner isotopolog  $^{13}\text{C}^{18}\text{O}$  to derive the  $\text{CO}$  column density. Using the  $^{12}\text{C}/^{13}\text{C}$  and  $^{16}\text{O}/^{18}\text{O}$  isotopic ratios, we obtained a column density for  $\text{CO}$  of  $1.5 \times 10^{19} \text{ cm}^{-2}$  (see Table B.1).

#### S 1.6. Diazenylium ( $\text{N}_2\text{H}^+$ )

The pattern of hyperfine transitions of  $\text{N}_2\text{H}^+ 1 \rightarrow 0$  is detected (see Fig. S 6). We fitted the hyperfine components using the HFS entry of CDMS. The transitions are optically thin ( $\tau < 0.21$ , see Table S 1). The obtained column density is  $6.7 \times 10^{13} \text{ cm}^{-2}$  (Table B.1).

#### S 1.7. Methanimine ( $\text{H}_2\text{CNH}$ )

We detected the low-energy  $4_{0,4} \rightarrow 3_{1,3}$  transitions of  $\text{H}_2\text{CNH}$ , which appear unblended (see Fig. S 7). The transition is optically thin ( $\tau = 0.015$ , see Table S 1). Fitting the excitation temperature to 20 K, the derived column density is  $1.8 \times 10^{14} \text{ cm}^{-2}$  (Table B.1).

#### S 1.8. Oxomethylium ( $\text{HCO}^+$ )

The  $1 \rightarrow 0$  transition of the main isotopolog of  $\text{HCO}^+$  is affected by absorption, due to filtering of extended emission and/or infall (see Fig. S 8). Therefore to obtain a reliable column density, we used an isotopolog. The  $\text{HC}^{17}\text{O}^+$  isotopolog is not detected, and hence we derived an upper limit (Table B.1). The transitions of  $\text{H}^{13}\text{CO}^+$  and  $\text{HC}^{18}\text{O}^+$  are detected, and appear unblended (Fig. S 8). We used  $\text{HC}^{18}\text{O}^+$  because it is optically thinner (see Table S 1). Using the  $^{16}\text{O}/^{18}\text{O}$  ratio we derived a  $\text{HCO}^+$  column density of  $1.1 \times 10^{15} \text{ cm}^{-2}$  (Table B.1).

### S 1.9. Formaldehyde ( $H_2CO$ )

The  $6_{1,5} \rightarrow 6_{1,6}$  transition of  $H_2CO$  is detected (see Fig. S 9). Using a fixed temperature of 20 K, we obtained a column density of  $1.4 \times 10^{15} \text{ cm}^{-2}$  (Table B.1), and an opacity of  $\tau = 0.019$  (Table S 1).

### S 1.10. Methanol ( $CH_3OH$ )

Several transitions of  $CH_3OH$ , shown in Fig. S 10, are detected. For this molecule, the addition of a second broader component was needed to properly fit the observed line profiles, which present high velocity wings. The transitions are optically thin, except the  $2_{0,2,0} \rightarrow 1_{0,1,0}$  transition, which is slightly optically thick ( $\tau = 0.52$  and  $\tau = 0.32$  for the broad and narrow component respectively, see Table S 1). The  $T_{\text{ex}}$  derived for the narrow and broad components converge to  $20.5 \pm 1.8$  K and  $9.9 \pm 0.9$  K, respectively (Table B.1). We derived column densities of  $3.5$  and  $3.8 \times 10^{15} \text{ cm}^{-2}$  for the narrow and broad components, respectively.

### S 1.11. Cyclopropenylidene ( $c\text{-}C_3H_2$ )

The  $2_{1,2,0} \rightarrow 1_{0,1,0}$  transition is clearly detected (see Fig. S 11). Using a fixed value of  $T_{\text{ex}} = 20$  K, the fit provides a line opacity of  $\tau = 0.09$  (see Table S 1). We also searched for the  $^{13}\text{C}$  isotopologs, but they are not detected. We thus consider the value for the column density obtained from the main isotopolog, which is  $5.0 \times 10^{13} \text{ cm}^{-2}$ .

### S 1.12. Propyne ( $CH_3CCH$ )

The  $K$  ladders of the  $J = 5 \rightarrow 4$  and  $J = 6 \rightarrow 5$  rotational transitions of  $CH_3CCH$  are detected (see Fig. S 12). The fit provides  $T_{\text{ex}} = 37 \pm 3$  K, and  $N = 8.6 \times 10^{14} \text{ cm}^{-2}$  (Table B.1), and low line opacities ( $\tau < 0.046$ , see Table S 1).

### S 1.13. Methyl cyanide ( $CH_3CN$ )

The  $K$  ladders of the  $J = 5 \rightarrow 4$  and  $J = 6 \rightarrow 5$  rotational transitions of  $CH_3CN$  are detected (Fig. S 13). The fit provides  $T_{\text{ex}} = 58 \pm 3$  K, and  $N = 2.4 \times 10^{14} \text{ cm}^{-2}$  (Table B.1), and low line opacities ( $\tau < 0.054$ , see Table S 1).

### S 1.14. Cyanamide ( $NH_2CN$ )

The  $5_{1,5,0} \rightarrow 4_{1,4,0}$  and  $5_{1,4,0} \rightarrow 4_{1,3,0}$  transitions are detected (Fig. S 14). Since both transitions have the same  $E_{\text{up}}$  (Table S 1), we fixed  $T_{\text{ex}}$  to 20 K, and obtained  $N = 5.0 \times 10^{12} \text{ cm}^{-2}$  (Table B.1).

### S 1.15. Ketene ( $H_2CCO$ )

The  $5_{1,5} \rightarrow 4_{1,4}$ ,  $5_{1,4} \rightarrow 4_{1,3}$ , and  $5_{0,5} \rightarrow 4_{0,4}$  transitions are detected (Fig. S 15). Using a fixed value of  $T_{\text{ex}} = 20$  K we derived a column density of  $7.1 \times 10^{13} \text{ cm}^{-2}$  (Table B.1), and optically thin lines ( $\tau < 0.019$ , see Table S 1).

### S 1.16. Isocyanic acid ( $HNCO$ )

Multiple  $5_{0,5,X} \rightarrow 4_{0,4,X}$  and  $4_{0,4,X} \rightarrow 3_{0,3,X}$  transitions (see Table S 1) are detected, as shown in Fig. S 16. The fit provides  $T_{\text{ex}} = 15.0 \pm 1.6$  K, and  $N = 2.6 \times 10^{14} \text{ cm}^{-2}$  (Table B.1).

### S 1.17. Acetaldehyde ( $CH_3CHO$ )

Multiple transitions of this molecule, shown in Fig. 2, are detected, covering a wide range of  $E_{\text{up}}$  (see Table S 1), which allows to properly constrain the excitation temperature. We derived  $T_{\text{ex}} = 13.3 \pm 0.8$  K, and  $N = 2.0 \times 10^{14} \text{ cm}^{-2}$  (Table B.1). The transitions are optically thin ( $\tau < 0.070$ , see Table S 1).

### S 1.18. Carbon monosulfide ( $CS$ )

The  $CS\ 2 \rightarrow 1$  rotational transition shows an absorption profile probably due to filtering of extended emission and/or infall, which prevents us to perform the fit (Fig. S 17). Multiple isotopologs are also detected:  $^{13}\text{CS}$ ,  $\text{C}^{33}\text{S}$ ,  $\text{C}^{34}\text{S}$ ,  $\text{C}^{36}\text{S}$  and  $^{13}\text{C}^{34}\text{S}$ , as shown in Fig. S 17. Since the spectral setup only covers a single rotational transition, we fixed  $T_{\text{ex}}$  to 20 K.  $^{13}\text{CS}$  and  $\text{C}^{34}\text{S}$  isotopologs are optically thick ( $\tau = 0.32$  and  $0.38$  respectively, see Table S 1), while  $\text{C}^{33}\text{S}$  has a slightly lower line opacity ( $\tau = 0.24$ ). Despite both remaining isotopologs being optically thin ( $\tau \sim 0.01$ ), we choose  $\text{C}^{36}\text{S}$  over  $^{13}\text{C}^{34}\text{S}$  to obtain the column density of the main molecule because the resultant column density of  $CS$  is slightly higher (a factor of 1.5) using  $\text{C}^{36}\text{S}$ . Finally, we apply the  $^{32}\text{S}/^{34}\text{S}$  and  $^{34}\text{S}/^{36}\text{S}$  isotopic ratios to the  $\text{C}^{36}\text{S}$  isotopolog, thus we obtained a  $CS$  column density of  $9 \times 10^{15} \text{ cm}^{-2}$ .

### S 1.19. Formamide ( $\text{NH}_2\text{CHO}$ )

The transitions of  $\text{NH}_2\text{CHO}$  are unblended, except for the  $5_{0,5,X} \rightarrow 4_{0,4,X}$  and  $5_{1,4,X} \rightarrow 4_{1,3,X}$  transitions which are contaminated with an unidentified species, nevertheless, they help to reproduce the observed spectrum (see Fig. 3). The FWHM is fixed to  $6.5 \text{ km s}^{-1}$  (see Table B.1), obtaining an optically thin LTE fit ( $\tau < 0.014$ ; see Table S 1). We derive a column density of  $2.63 \times 10^{13} \text{ cm}^{-2}$  for  $\text{NH}_2\text{CHO}$ .

### S 1.20. Thiomethylum ( $\text{HCS}^+$ )

The only  $2 \rightarrow 1$   $\text{HCS}^+$  transition is detected (see Fig. S 18). The temperature is fixed to 20K (see Table B.1) because there is only one transition available. The fit provides optically thin transitions ( $\tau = 0.061$ , see Table S 1) and a resultant column density of  $3.1 \times 10^{13} \text{ cm}^{-2}$ .

### S 1.21. Thioformaldehyde ( $\text{H}_2\text{CS}$ )

Three  $\text{H}_2\text{CS}$  transitions are detected (see Fig. S 19). Due to the broader line profile and high velocity wings, we use two components to perform the fit. The obtained fit have a temperature of  $25 \pm 4 \text{ K}$  and  $69 \pm 24 \text{ K}$  for the narrow and broad component, respectively (see Table B.1). The resultant the LTE fit have optically thin transitions ( $\tau < 0.099$ , see Table S 1). We obtained a column density of 0.19 (narrow) and 1.3 (broad)  $\times 10^{15} \text{ cm}^{-2}$  for each component.

### S 1.22. Dimethyl ether ( $\text{CH}_3\text{OCH}_3$ )

The multiple  $\text{CH}_3\text{OCH}_3$  transitions are detected (see Fig. S 20) and the  $4_{2,3,X} \rightarrow 4_{1,4,X}$  transitions despite their faintness, they contribute to reproduce the observed spectrum. The FWHM is fixed to  $6.5 \text{ km s}^{-1}$  (see Table B.1), the transitions of the resultant fit are optically thin ( $\tau < 0.009$ , see Table S 1) and the derived column density of  $\text{CH}_3\text{OCH}_3$  is  $3.8 \times 10^{14} \text{ cm}^{-2}$ .

### S 1.23. Nitrogen Sulfide (NS)

The  $3_{1,3,X} \rightarrow 2_{-1,2,X}$  and  $3_{-1,3,X} \rightarrow 2_{1,2,X}$  transitions are detected (see Fig. S 21). We fixed the temperature to  $T = 20 \text{ K}$  (see Table B.1) because the energy of the transitions is very similar ( $E_{\text{up}} \sim 8.8 \text{ K}$ ). The fit that we obtained has optically thin transitions ( $\tau < 0.096$ , see Table S 1) and the column density is  $2.5 \times 10^{14} \text{ cm}^{-2}$ .

### S 1.24. Ethanol ( $\text{C}_2\text{H}_5\text{OH}$ )

The multiple  $\text{C}_2\text{H}_5\text{OH}$  transitions are detected (see Fig. S 22). We perform the LTE fit obtaining  $T_{\text{ex}} = 23 \pm 4 \text{ K}$  (see Table B.1) and optically thin lines ( $\tau < 0.009$ , see Table S 1). We obtained a column density of  $3.4 \times 10^{14} \text{ cm}^{-2}$ .

### S 1.25. Methyl mercaptan ( $\text{CH}_3\text{SH}$ )

The  $\text{CH}_3\text{SH}$  transitions are unblended except for the  $4_{1,3,1} \rightarrow 3_{1,2,1}$  transition, which is slightly blended with  $\text{H}_2\text{C}^{34}\text{S}$  (see Fig. 4). We perform the fit and we obtained optically thin lines ( $\tau < 0.032$ , see Table S 1). The resultant column density of the fit is  $1.3 \times 10^{14} \text{ cm}^{-2}$ .

### S 1.26. Cyanoacetylene ( $\text{HC}_3\text{N}$ )

The three  $\text{HC}_3\text{N}$  transitions are detected (see Fig. S 23). We add a second component to fit this molecule due to the broadening of the line profile and the high velocity wings. However, the fit provides us with slightly optically thick lines ( $\tau < 0.23$ , see Table S 1). Therefore, we search for isotopologs and we detected three (see Fig. S 23):  $\text{H}^{13}\text{CCCN}$ ,  $\text{HC}^{13}\text{CCN}$  and  $\text{HCC}^{13}\text{CN}$ . Two out of three transitions of  $\text{HCC}^{13}\text{CN}$  are not well fitted. Thus, we will use the  $\text{H}^{13}\text{CCCN}$  and  $\text{HC}^{13}\text{CCN}$  isotopologs to obtain  $\text{HC}_3\text{N}$  column density. The only blended transition of both isotopologs is the  $11 \rightarrow 10$  of  $\text{H}^{13}\text{CCCN}$  which is blended with  $\text{CH}_3\text{CN}$ . The FWHM of  $\text{H}^{13}\text{CCCN}$  and  $\text{HCC}^{13}\text{CN}$  is fixed to  $4.5 \text{ km s}^{-1}$  which is the value that converged for the  $\text{HC}^{13}\text{CCN}$  isotopolog (see Table B.1). The fit shows that they are also optically thin ( $\tau < 0.011$ ). Thus, we used the column densities of  $\text{H}^{13}\text{CCCN}$  and  $\text{HC}^{13}\text{CCN}$  to obtain the value for  $\text{HC}_3\text{N}$ . Using the  $^{12}\text{C}/^{13}\text{C}$  ratio, we derive a column density of  $1.5 \times 10^{14} \text{ cm}^{-2}$ .

### S 1.27. Vinyl cyanide ( $\text{C}_2\text{H}_3\text{CN}$ )

Several  $\text{C}_2\text{H}_3\text{CN}$  transitions are detected (see Fig. S 24). There are only two blended transitions:  $10_{0,10} \rightarrow 9_{0,9}$  and  $10_{1,9} \rightarrow 9_{1,8}$  with  $\text{C}_2\text{H}_5\text{OH}$  and  $\text{H}^{13}\text{CCCN}$ , respectively, and they help to reproduce the observational spectrum. We fixed the FWHM to  $6.5 \text{ km s}^{-1}$  (see Table B.1) and the transitions of the fit are optically thin ( $\tau < 0.031$ , see Table S 1). The column density for  $\text{C}_2\text{H}_3\text{CN}$  is  $3.2 \times 10^{13} \text{ cm}^{-2}$ .

### S 1.28. Methyl formate ( $\text{CH}_3\text{OCHO}$ )

Multiple  $\text{CH}_3\text{OCHO}$  transitions are detected (see Fig. S 25). The excitation temperature of the fit is  $26 \pm 12$  K (see Table B.1) and the transitions are optically thin ( $\tau < 0.003$ , see Table S 1). The column density obtained is  $1.3 \times 10^{14} \text{ cm}^{-2}$ .

### S 1.29. Carbonyl sulfide (OCS)

Three transitions of OCS are detected (see Fig. S 26). To reproduce the broad line profile, we add a second component to the fit. We fix the temperature of the narrow component (see Table B.1) and the transitions of the resultant fit are optically thin ( $\tau < 0.13$ , see Table S 1). We obtained these column densities for each component, 8.3 (narrow) and 10.8 (broad)  $\times 10^{14} \text{ cm}^{-2}$ .

### S 1.30. Cyanodiacetylene ( $\text{HC}_5\text{N}$ )

Several  $\text{HC}_5\text{N}$  transitions are detected (see Fig. S 27). The fit converged, the transitions are optically thin ( $\tau < 0.005$ , see Table S 1) and the obtained temperature is  $T_{\text{ex}} = 38 \pm 12$  K. The resultant column density is  $1 \times 10^{13} \text{ cm}^{-2}$ .

## S 2. Molecular transitions used in the analysis

The transitions used to perform the fits of the analyzed species toward G31.41+0.31 shock and core are listed in Table S 1 and S 2, respectively. The transitions of G31.41 shock are plotted in Appendices S 3 and S 4, and those of G31.41 core are depicted in Appendices S 7 and S 8.

Table S 1: List of the transitions of the molecules analyzed in this work in G31.41 shock that were used to perform the MADCUBA fits (depicted in Table B.1 and B.2), ordered by increasing molecular mass.

Molecule	Frequency (GHz)	Transition	$\log I$ ( $\text{nm}^2 \text{ MHz}$ )	$E_{\text{up}}$ (K)	Area ( $\text{K km s}^{-1}$ )	$\tau$
Detected molecules						
$\text{NH}_2\text{D}$	85.92628	$1_{1,1,0} \rightarrow 1_{0,1,1}$	-3.4580	20.679	$5.00 \pm 0.17$	$0.088 \pm 0.007$
$\text{NH}_2\text{D}$	85.92628	$1_{1,1,0} \rightarrow 1_{0,1,1}$	-3.4580	20.679	$1.51 \pm 0.15$	$0.035 \pm 0.007$
$\text{NH}_2\text{D}$	110.15359	$1_{1,1,1} \rightarrow 1_{0,1,0}$	-3.7187	21.259	$2.14 \pm 0.17$	$0.038 \pm 0.007$
$\text{NH}_2\text{D}$	110.15359	$1_{1,1,1} \rightarrow 1_{0,1,0}$	-3.7187	21.259	$0.64 \pm 0.15$	$0.015 \pm 0.007$
CCH	87.28410	$1_{2,1} \rightarrow 0_{1,1}$	-5.2060	4.1911	$1.2 \pm 0.2$	$0.04 \pm 0.03$
CCH	87.31690	$1_{2,2} \rightarrow 0_{1,1}$	-4.2140	4.1927	$10.2 \pm 0.2$	$0.4 \pm 0.2$
CCH	87.32859	$1_{2,1} \rightarrow 0_{1,0}$	-4.5166	4.1911	$5.4 \pm 0.2$	$0.20 \pm 0.11$
CCH	87.40199	$1_{1,1} \rightarrow 0_{1,1}$	-4.5159	4.1968	$5.4 \pm 0.2$	$0.20 \pm 0.11$
CCH	87.40716	$1_{1,0} \rightarrow 0_{1,1}$	-4.9121	4.1970	$2.3 \pm 0.2$	$0.08 \pm 0.04$
CCH	87.44647	$1_{1,1} \rightarrow 0_{1,0}$	-5.2044	4.1968	$1.2 \pm 0.2$	$0.04 \pm 0.03$
$\text{H}^{13}\text{CN}$	86.33873	$1_1 \rightarrow 0_1$	-3.0246	4.1436	$9.6 \pm 1.1$	$0.08 \pm 0.03$
$\text{H}^{13}\text{CN}$	86.34016	$1_2 \rightarrow 0_1$	-2.8027	4.1437	$15.8 \pm 1.1$	$0.13 \pm 0.03$
$\text{H}^{13}\text{CN}$	86.34225	$1_0 \rightarrow 0_1$	-3.5017	4.1438	$3.3 \pm 1.1$	$0.03 \pm 0.03$
$\text{HC}^{15}\text{N}$	86.05497	$1 \rightarrow 0$	-2.5525	4.1300	$4.4 \pm 0.3$	$0.056 \pm 0.012$
$\text{H}^{15}\text{NC}$	88.86571	$1 \rightarrow 0$	-2.5690	4.2649	$0.46 \pm 0.05$	$(8.5 \pm 1.9) \cdot 10^{-3}$
$\text{HN}^{13}\text{C}$	87.09083	$1 \rightarrow 0$	-2.4894	4.1797	$4.44 \pm 0.16$	$0.090 \pm 0.007$
$\text{C}^{17}\text{O}$	112.35878	$1_2 \rightarrow 0_3$	-5.6952	5.3924	$2.07 \pm 0.17$	$0.39 \pm 0.13$
$\text{C}^{17}\text{O}$	112.35898	$1_4 \rightarrow 0_3$	-5.3942	5.3924	$3.70 \pm 0.18$	$0.8 \pm 0.3$
$\text{C}^{17}\text{O}$	112.36001	$1_3 \rightarrow 0_3$	-5.5191	5.3924	$2.94 \pm 0.18$	$0.59 \pm 0.19$
$\text{C}^{18}\text{O}$	109.78217	$1 \rightarrow 0$	-5.0708	5.2687	$29.3 \pm 0.7$	$0.93 \pm 0.08$
$^{13}\text{C}^{18}\text{O}$	104.71140	$1_2 \rightarrow 0_1$	-5.3069	5.0254	$0.52 \pm 0.11$	$0.013 \pm 0.005$
$^{13}\text{C}^{18}\text{O}$	104.71140	$1_1 \rightarrow 0_1$	-5.6079	5.0254	$0.26 \pm 0.11$	$(6 \pm 5) \cdot 10^{-3}$
$\text{N}_2\text{H}^+$	93.17162	$1_{1,0} \rightarrow 0_{1,1}$	-3.7697	4.4715	$1.3 \pm 1.8$	$0.03 \pm 0.09$
$\text{N}_2\text{H}^+$	93.17191	$1_{1,2} \rightarrow 0_{1,2}$	-3.1439	4.4715	$5.2 \pm 1.8$	$0.13 \pm 0.09$
$\text{N}_2\text{H}^+$	93.17191	$1_{1,2} \rightarrow 0_{1,1}$	-3.8803	4.4715	$1.0 \pm 1.8$	$0.02 \pm 0.09$
$\text{N}_2\text{H}^+$	93.17205	$1_{1,1} \rightarrow 0_{1,0}$	-3.5859	4.4715	$1.9 \pm 1.8$	$0.05 \pm 0.09$
$\text{N}_2\text{H}^+$	93.17205	$1_{1,1} \rightarrow 0_{1,2}$	-3.7225	4.4715	$1.4 \pm 1.8$	$0.03 \pm 0.09$
$\text{N}_2\text{H}^+$	93.17205	$1_{1,1} \rightarrow 0_{1,1}$	-4.2155	4.4715	$0.5 \pm 1.8$	$0.01 \pm 0.08$
$\text{N}_2\text{H}^+$	93.17347	$1_{2,2} \rightarrow 0_{1,1}$	-3.1439	4.4716	$5.2 \pm 1.8$	$0.13 \pm 0.09$
$\text{N}_2\text{H}^+$	93.17347	$1_{2,2} \rightarrow 0_{1,2}$	-3.8803	4.4716	$1.0 \pm 1.8$	$0.02 \pm 0.09$
$\text{N}_2\text{H}^+$	93.17377	$1_{2,3} \rightarrow 0_{1,2}$	-2.9246	4.4716	$8.4 \pm 1.8$	$0.21 \pm 0.10$
$\text{N}_2\text{H}^+$	93.17396	$1_{2,1} \rightarrow 0_{1,1}$	-3.4811	4.4716	$2.5 \pm 1.8$	$0.06 \pm 0.09$
$\text{N}_2\text{H}^+$	93.17396	$1_{2,1} \rightarrow 0_{1,0}$	-3.7972	4.4716	$1.2 \pm 1.8$	$0.03 \pm 0.09$
$\text{N}_2\text{H}^+$	93.17396	$1_{2,1} \rightarrow 0_{1,2}$	-4.6978	4.4716	$0.2 \pm 1.8$	$0.00 \pm 0.08$
$\text{N}_2\text{H}^+$	93.17626	$1_{0,1} \rightarrow 0_{1,2}$	-3.5224	4.4718	$2.2 \pm 1.8$	$0.05 \pm 0.09$

Table S 1: Continued.

Molecule	Frequency (GHz)	Transition	$\log I$ ( $\text{nm}^2 \text{ MHz}$ )	$E_{\text{up}}$ (K)	Area ( $\text{K km s}^{-1}$ )	$\tau$
$\text{N}_2\text{H}^+$	93.17626	$1_{0,1} \rightarrow 0_{1,1}$	-3.9256	4.4718	$0.9 \pm 1.8$	$0.02 \pm 0.09$
$\text{N}_2\text{H}^+$	93.17626	$1_{0,1} \rightarrow 0_{1,0}$	-4.0417	4.4718	$0.7 \pm 1.8$	$0.02 \pm 0.08$
$\text{H}_2\text{CNH}$	105.79406	$4_{0,4} \rightarrow 3_{1,3}$	-3.9162	30.619	$2.34 \pm 0.09$	$0.015 \pm 0.002$
$\text{H}^{13}\text{CO}^+$	86.75429	$1 \rightarrow 0$	-2.2808	4.1635	$6.22 \pm 0.19$	$0.138 \pm 0.010$
$\text{HC}^{18}\text{O}^+$	85.16222	$1 \rightarrow 0$	-2.3049	4.0871	$1.88 \pm 0.17$	$0.042 \pm 0.008$
$\text{H}_2\text{CO}$	101.33299	$6_{1,5} \rightarrow 6_{1,6}$	-4.0441	87.564	$1.06 \pm 0.12$	$0.019 \pm 0.005$
$\text{CH}_3\text{OH}$	85.56813	$6_{2,4,2} \rightarrow 7_{1,7,2}$	-5.0811	74.657	$1.1 \pm 0.5$	$0.013 \pm 0.017$
$\text{CH}_3\text{OH}$	85.56813	$6_{2,4,2} \rightarrow 7_{1,7,2}$	-5.0811	74.657	$0.1 \pm 1.1$	$0.00 \pm 0.04$
$\text{CH}_3\text{OH}$	95.91431	$2_{1,2,0} \rightarrow 1_{1,1,0}$	-5.1228	21.444	$9.6 \pm 0.5$	$0.12 \pm 0.02$
$\text{CH}_3\text{OH}$	95.91431	$2_{1,2,0} \rightarrow 1_{1,1,0}$	-5.1228	21.444	$11.9 \pm 1.1$	$0.09 \pm 0.05$
$\text{CH}_3\text{OH}$	96.73936	$2_{1,2,2} \rightarrow 1_{1,1,2}$	-5.1027	12.5411	$28.2 \pm 1.1$	$0.22 \pm 0.06$
$\text{CH}_3\text{OH}$	96.73936	$2_{1,2,2} \rightarrow 1_{1,1,2}$	-5.1027	12.5411	$14.7 \pm 0.5$	$0.18 \pm 0.03$
$\text{CH}_3\text{OH}$	96.74137	$2_{0,2,0} \rightarrow 1_{0,1,0}$	-4.9699	6.9643	$60.3 \pm 1.1$	$0.52 \pm 0.10$
$\text{CH}_3\text{OH}$	96.74137	$2_{0,2,0} \rightarrow 1_{0,1,0}$	-4.9699	6.9643	$24.7 \pm 0.5$	$0.32 \pm 0.04$
$\text{CH}_3\text{OH}$	96.74455	$2_{0,2,1} \rightarrow 1_{0,1,1}$	-4.9890	20.089	$13.6 \pm 0.5$	$0.17 \pm 0.03$
$\text{CH}_3\text{OH}$	96.74455	$2_{0,2,1} \rightarrow 1_{0,1,1}$	-4.9890	20.089	$18.0 \pm 1.1$	$0.14 \pm 0.05$
$\text{CH}_3\text{OH}$	96.75550	$2_{1,1,1} \rightarrow 1_{1,0,1}$	-5.1139	28.011	$7.3 \pm 0.5$	$0.09 \pm 0.02$
$\text{CH}_3\text{OH}$	96.75550	$2_{1,1,1} \rightarrow 1_{1,0,1}$	-5.1139	28.011	$6.4 \pm 1.1$	$0.05 \pm 0.05$
$\text{CH}_3\text{OH}$	97.58280	$2_{1,1,0} \rightarrow 1_{1,0,0}$	-5.1079	21.564	$9.8 \pm 0.5$	$0.12 \pm 0.02$
$\text{CH}_3\text{OH}$	97.58280	$2_{1,1,0} \rightarrow 1_{1,0,0}$	-5.1079	21.564	$12.0 \pm 1.1$	$0.09 \pm 0.05$
$\text{CH}_3\text{OH}$	107.01383	$3_{1,3,0} \rightarrow 4_{0,4,0}$	-4.6431	28.348	$18.5 \pm 0.5$	$0.24 \pm 0.03$
$\text{CH}_3\text{OH}$	107.01383	$3_{1,3,0} \rightarrow 4_{0,4,0}$	-4.6431	28.348	$16.4 \pm 1.1$	$0.13 \pm 0.05$
$\text{CH}_3\text{OH}$	108.89395	$0_{0,0,1} \rightarrow 1_{1,1,2}$	-5.0938	13.1245	$24.7 \pm 1.1$	$0.20 \pm 0.06$
$\text{CH}_3\text{OH}$	108.89395	$0_{0,0,1} \rightarrow 1_{1,1,2}$	-5.0938	13.1245	$13.1 \pm 0.5$	$0.17 \pm 0.03$
$\text{CH}_3\text{OH}$	111.28945	$7_{2,5,0} \rightarrow 8_{1,8,0}$	-4.8266	102.715	$0.4 \pm 0.5$	$0.005 \pm 0.018$
$\text{CH}_3\text{OH}$	111.28945	$7_{2,5,0} \rightarrow 8_{1,8,0}$	-4.8266	102.715	$0.0 \pm 1.1$	$0.00 \pm 0.05$
$\text{c-C}_3\text{H}_2$	85.33889	$2_{1,2,0} \rightarrow 1_{0,1,0}$	-3.7184	6.4454	$3.99 \pm 0.16$	$0.089 \pm 0.008$
$\text{CH}_3\text{CCH}$	85.44260	$5_3 \rightarrow 4_3$	-4.7776	77.336	$0.87 \pm 0.13$	$(8 \pm 3) \cdot 10^{-3}$
$\text{CH}_3\text{CCH}$	85.45077	$5_2 \rightarrow 4_2$	-4.9082	41.210	$1.51 \pm 0.13$	$0.014 \pm 0.003$
$\text{CH}_3\text{CCH}$	85.45567	$5_1 \rightarrow 4_1$	-4.8187	19.5308	$3.09 \pm 0.13$	$0.028 \pm 0.004$
$\text{CH}_3\text{CCH}$	85.45730	$5_0 \rightarrow 4_0$	-4.7905	12.3040	$3.90 \pm 0.13$	$0.036 \pm 0.004$
$\text{CH}_3\text{CCH}$	102.53035	$6_3 \rightarrow 5_3$	-4.4777	82.257	$1.29 \pm 0.13$	$0.012 \pm 0.003$
$\text{CH}_3\text{CCH}$	102.54014	$6_2 \rightarrow 5_2$	-4.6526	46.131	$2.03 \pm 0.13$	$0.019 \pm 0.003$
$\text{CH}_3\text{CCH}$	102.54602	$6_1 \rightarrow 5_1$	-4.5822	24.452	$3.96 \pm 0.13$	$0.037 \pm 0.004$
$\text{CH}_3\text{CCH}$	102.54798	$6_0 \rightarrow 5_0$	-4.5595	17.2254	$4.93 \pm 0.13$	$0.046 \pm 0.005$
$\text{CH}_3\text{CN}$	91.95873	$5_{4,0} \rightarrow 4_{4,0}$	-3.8674	127.541	$0.9 \pm 0.4$	$(2 \pm 3) \cdot 10^{-3}$
$\text{CH}_3\text{CN}$	91.97113	$5_{-3,0} \rightarrow 4_{3,0}$	-3.5450	77.545	$3.9 \pm 0.4$	$(8 \pm 4) \cdot 10^{-3}$
$\text{CH}_3\text{CN}$	91.97113	$5_{3,0} \rightarrow 4_{-3,0}$	-3.5450	77.545	$3.9 \pm 0.4$	$(8 \pm 4) \cdot 10^{-3}$
$\text{CH}_3\text{CN}$	91.97999	$5_{2,0} \rightarrow 4_{2,0}$	-3.3752	41.825	$9.5 \pm 0.4$	$0.021 \pm 0.004$
$\text{CH}_3\text{CN}$	91.98531	$5_{1,0} \rightarrow 4_{1,0}$	-3.2861	20.390	$15.7 \pm 0.4$	$0.034 \pm 0.004$
$\text{CH}_3\text{CN}$	91.98709	$5_{0,0} \rightarrow 4_{0,0}$	-3.2580	13.2441	$18.4 \pm 0.4$	$0.040 \pm 0.004$
$\text{CH}_3\text{CN}$	110.33035	$6_{5,0} \rightarrow 5_{5,0}$	-3.8013	197.098	$0.3 \pm 0.4$	$(1 \pm 4) \cdot 10^{-3}$
$\text{CH}_3\text{CN}$	110.34947	$6_{4,0} \rightarrow 5_{4,0}$	-3.4485	132.837	$1.9 \pm 0.4$	$(4 \pm 4) \cdot 10^{-3}$
$\text{CH}_3\text{CN}$	110.36435	$6_{-3,0} \rightarrow 5_{3,0}$	-3.2456	82.842	$6.0 \pm 0.4$	$0.013 \pm 0.004$
$\text{CH}_3\text{CN}$	110.36435	$6_{3,0} \rightarrow 5_{-3,0}$	-3.2456	82.842	$6.0 \pm 0.4$	$0.013 \pm 0.004$
$\text{CH}_3\text{CN}$	110.37499	$6_{2,0} \rightarrow 5_{2,0}$	-3.1201	47.122	$13.2 \pm 0.4$	$0.029 \pm 0.004$
$\text{CH}_3\text{CN}$	110.38137	$6_{1,0} \rightarrow 5_{1,0}$	-3.0501	25.687	$20.8 \pm 0.4$	$0.046 \pm 0.004$
$\text{CH}_3\text{CN}$	110.38350	$6_{0,0} \rightarrow 5_{0,0}$	-3.0275	18.5417	$24.2 \pm 0.4$	$0.054 \pm 0.005$
$\text{NH}_2\text{CN}$	99.31120	$5_{1,5,0} \rightarrow 4_{1,4,0}$	-3.0431	28.797	$1.05 \pm 0.09$	$(9 \pm 3) \cdot 10^{-3}$
$\text{NH}_2\text{CN}$	100.62950	$5_{1,4,0} \rightarrow 4_{1,3,0}$	-3.0319	28.987	$1.06 \pm 0.09$	$(9 \pm 3) \cdot 10^{-3}$
$\text{H}_2\text{CCO}$	100.09451	$5_{1,5} \rightarrow 4_{1,4}$	-3.7629	27.463	$1.69 \pm 0.13$	$0.019 \pm 0.004$
$\text{H}_2\text{CCO}$	101.03663	$5_{0,5} \rightarrow 4_{0,4}$	-4.1955	14.5474	$1.13 \pm 0.13$	$0.013 \pm 0.004$
$\text{H}_2\text{CCO}$	101.98143	$5_{1,4} \rightarrow 4_{1,3}$	-3.7471	27.735	$1.70 \pm 0.13$	$0.019 \pm 0.004$
$\text{HNCO}$	87.59656	$4_{1,4,3} \rightarrow 3_{1,3,3}$	-5.4785	53.785	$0.0 \pm 0.3$	$0.000 \pm 0.011$
$\text{HNCO}$	87.59734	$4_{1,4,5} \rightarrow 3_{1,3,4}$	-4.1872	53.785	$0.4 \pm 0.3$	$0.004 \pm 0.011$
$\text{HNCO}$	87.59734	$4_{1,4,4} \rightarrow 3_{1,3,3}$	-4.3024	53.785	$0.3 \pm 0.3$	$0.003 \pm 0.011$
$\text{HNCO}$	87.59734	$4_{1,4,3} \rightarrow 3_{1,3,2}$	-4.4205	53.785	$0.2 \pm 0.3$	$0.002 \pm 0.011$
$\text{HNCO}$	87.59799	$4_{1,4,4} \rightarrow 3_{1,3,4}$	-5.4785	53.785	$0.0 \pm 0.3$	$0.000 \pm 0.011$
$\text{HNCO}$	87.92438	$4_{0,4,3} \rightarrow 3_{0,3,3}$	-5.3846	10.5494	$0.4 \pm 0.3$	$0.003 \pm 0.011$

Table S 1: Continued.

Molecule	Frequency (GHz)	Transition	$\log I$ (nm <sup>2</sup> MHz)	$E_{\text{up}}$ (K)	Area (K km s <sup>-1</sup> )	$\tau$
HNCO	87.92504	4 <sub>0,4,3</sub> → 3 <sub>0,3,4</sub>	-7.1840	10.5493	0.0 ± 0.3	0.000 ± 0.011
HNCO	87.92525	4 <sub>0,4,5</sub> → 3 <sub>0,3,4</sub>	-4.0933	10.5493	7.6 ± 0.3	0.067 ± 0.014
HNCO	87.92525	4 <sub>0,4,4</sub> → 3 <sub>0,3,3</sub>	-4.2085	10.5494	5.9 ± 0.3	0.052 ± 0.013
HNCO	87.92525	4 <sub>0,4,3</sub> → 3 <sub>0,3,2</sub>	-4.3266	10.5493	4.5 ± 0.3	0.039 ± 0.012
HNCO	87.92590	4 <sub>0,4,4</sub> → 3 <sub>0,3,4</sub>	-5.3846	10.5493	0.4 ± 0.3	0.003 ± 0.011
HNCO	88.23849	4 <sub>1,3,3</sub> → 3 <sub>1,2,3</sub>	-5.4722	53.862	0.0 ± 0.3	0.000 ± 0.011
HNCO	88.23904	4 <sub>1,3,5</sub> → 3 <sub>1,2,4</sub>	-4.1809	53.862	0.4 ± 0.3	0.004 ± 0.011
HNCO	88.23904	4 <sub>1,3,4</sub> → 3 <sub>1,2,3</sub>	-4.2961	53.862	0.3 ± 0.3	0.003 ± 0.011
HNCO	88.23904	4 <sub>1,3,3</sub> → 3 <sub>1,2,2</sub>	-4.4142	53.862	0.2 ± 0.3	0.002 ± 0.011
HNCO	88.23951	4 <sub>1,3,4</sub> → 3 <sub>1,2,4</sub>	-5.4722	53.862	0.0 ± 0.3	0.000 ± 0.011
HNCO	109.90492	5 <sub>0,5,4</sub> → 4 <sub>0,4,4</sub>	-5.2946	15.8239	0.3 ± 0.3	0.003 ± 0.011
HNCO	109.90576	5 <sub>0,5,6</sub> → 4 <sub>0,4,5</sub>	-3.8241	15.8239	8.2 ± 0.3	0.074 ± 0.014
HNCO	109.90576	5 <sub>0,5,5</sub> → 4 <sub>0,4,4</sub>	-3.9143	15.8239	6.7 ± 0.3	0.060 ± 0.013
HNCO	109.90576	5 <sub>0,5,4</sub> → 4 <sub>0,4,3</sub>	-4.0058	15.8239	5.5 ± 0.3	0.049 ± 0.013
HNCO	109.90643	5 <sub>0,5,5</sub> → 4 <sub>0,4,5</sub>	-5.2945	15.8240	0.3 ± 0.3	0.003 ± 0.011
CH <sub>3</sub> CHO	93.58091	5 <sub>1,5,0</sub> → 4 <sub>1,4,0</sub>	-4.4093	15.7469	3.93 ± 0.14	0.057 ± 0.008
CH <sub>3</sub> CHO	93.59523	5 <sub>1,5,1</sub> → 4 <sub>1,4,1</sub>	-4.4093	15.8216	3.91 ± 0.14	0.057 ± 0.008
CH <sub>3</sub> CHO	95.94744	5 <sub>0,5,2</sub> → 4 <sub>0,4,2</sub>	-4.3672	13.9338	4.80 ± 0.14	0.070 ± 0.008
CH <sub>3</sub> CHO	95.96346	5 <sub>0,5,0</sub> → 4 <sub>0,4,0</sub>	-4.3672	13.8368	4.83 ± 0.14	0.070 ± 0.008
CH <sub>3</sub> CHO	96.27425	5 <sub>2,4,0</sub> → 4 <sub>2,3,0</sub>	-4.4528	22.934	2.09 ± 0.14	0.030 ± 0.007
CH <sub>3</sub> CHO	96.36779	5 <sub>3,3,0</sub> → 4 <sub>3,2,0</sub>	-4.5863	34.256	0.69 ± 0.14	(10 ± 7) · 10 <sup>-3</sup>
CH <sub>3</sub> CHO	96.36837	5 <sub>3,2,2</sub> → 4 <sub>3,1,2</sub>	-4.5863	34.260	0.69 ± 0.14	(10 ± 7) · 10 <sup>-3</sup>
CH <sub>3</sub> CHO	96.37179	5 <sub>3,2,0</sub> → 4 <sub>3,1,0</sub>	-4.5863	34.256	0.69 ± 0.14	(10 ± 7) · 10 <sup>-3</sup>
CH <sub>3</sub> CHO	96.42561	5 <sub>2,4,1</sub> → 4 <sub>2,3,1</sub>	-4.4539	22.911	2.08 ± 0.14	0.030 ± 0.007
CH <sub>3</sub> CHO	96.47552	5 <sub>2,3,2</sub> → 4 <sub>2,2,2</sub>	-4.4535	23.025	2.07 ± 0.14	0.030 ± 0.007
CH <sub>3</sub> CHO	96.63266	5 <sub>2,3,0</sub> → 4 <sub>2,2,0</sub>	-4.4496	22.964	2.09 ± 0.14	0.030 ± 0.007
CH <sub>3</sub> CHO	98.86331	5 <sub>1,4,2</sub> → 4 <sub>1,3,2</sub>	-4.3627	16.5889	3.92 ± 0.14	0.057 ± 0.008
CH <sub>3</sub> CHO	98.90094	5 <sub>1,4,0</sub> → 4 <sub>1,3,0</sub>	-4.3622	16.5133	3.94 ± 0.14	0.057 ± 0.008
CH <sub>3</sub> CHO	112.24872	6 <sub>1,6,0</sub> → 5 <sub>1,5,0</sub>	-4.1738	21.134	3.89 ± 0.14	0.057 ± 0.008
CH <sub>3</sub> CHO	112.25451	6 <sub>1,6,1</sub> → 5 <sub>1,5,1</sub>	-4.1737	21.209	3.87 ± 0.14	0.057 ± 0.008
CH <sub>3</sub> CHO	114.94017	6 <sub>0,6,2</sub> → 5 <sub>0,5,2</sub>	-4.1386	19.4500	4.64 ± 0.14	0.069 ± 0.008
CH <sub>3</sub> CHO	114.95990	6 <sub>0,6,0</sub> → 5 <sub>0,5,0</sub>	-4.1386	19.3539	4.67 ± 0.14	0.069 ± 0.008
CH <sub>3</sub> CHO	115.49392	6 <sub>2,5,0</sub> → 5 <sub>2,4,0</sub>	-4.1984	28.477	2.13 ± 0.14	0.031 ± 0.007
CH <sub>3</sub> CHO	115.69505	6 <sub>2,5,1</sub> → 5 <sub>2,4,1</sub>	-4.2029	28.464	2.11 ± 0.14	0.031 ± 0.007
CH <sub>3</sub> CHO	115.91032	6 <sub>2,4,2</sub> → 5 <sub>2,3,2</sub>	-4.2014	28.588	2.10 ± 0.14	0.031 ± 0.007
<sup>13</sup> CS	92.49431	2 → 1	-2.7959	6.6586	13.2 ± 0.3	0.317 ± 0.019
<sup>13</sup> CS	92.49431	2 → 1	-2.7959	6.6586	33.2 ± 0.5	0.289 ± 0.019
C <sup>33</sup> S	97.16629	2 <sub>0,1</sub> → 1 <sub>0,2</sub>	-4.5142	6.9952	0.5 ± 0.2	0.010 ± 0.015
C <sup>33</sup> S	97.16951	2 <sub>0,2</sub> → 1 <sub>0,2</sub>	-3.7080	6.9953	2.9 ± 0.2	0.06 ± 0.03
C <sup>33</sup> S	97.17184	2 <sub>0,4</sub> → 1 <sub>0,3</sub>	-3.1340	6.9953	10.2 ± 0.2	0.24 ± 0.12
C <sup>33</sup> S	97.17184	2 <sub>0,3</sub> → 1 <sub>0,2</sub>	-3.4138	6.9955	5.6 ± 0.2	0.13 ± 0.06
C <sup>33</sup> S	97.17184	2 <sub>0,1</sub> → 1 <sub>0,1</sub>	-3.8152	6.9952	2.3 ± 0.2	0.05 ± 0.03
C <sup>33</sup> S	97.17262	2 <sub>0,2</sub> → 1 <sub>0,3</sub>	-4.7360	6.9954	0.3 ± 0.2	0.006 ± 0.014
C <sup>33</sup> S	97.17500	2 <sub>0,3</sub> → 1 <sub>0,3</sub>	-3.7818	6.9955	2.4 ± 0.2	0.05 ± 0.03
C <sup>33</sup> S	97.17527	2 <sub>0,2</sub> → 1 <sub>0,1</sub>	-3.8152	6.9953	2.3 ± 0.2	0.05 ± 0.03
C <sup>34</sup> S	96.41295	2 <sub>0</sub> → 1 <sub>0</sub>	-2.7462	6.9406	17.4 ± 0.4	0.38 ± 0.02
C <sup>34</sup> S	96.41295	2 <sub>0</sub> → 1 <sub>0</sub>	-2.7462	6.9406	47.7 ± 0.6	0.35 ± 0.02
<sup>13</sup> C <sup>34</sup> S	90.92603	2 → 1	-2.8223	6.5456	1.29 ± 0.08	0.014 ± 0.003
C <sup>36</sup> S	95.01672	2 <sub>80</sub> → 1 <sub>80</sub>	-2.7651	6.8401	0.75 ± 0.07	0.011 ± 0.003
NH <sub>2</sub> CHO	84.54142	4 <sub>0,4,3</sub> → 3 <sub>0,3,3</sub>	-5.2848	10.1571	0.06 ± 0.17	(1 ± 6) · 10 <sup>-3</sup>
NH <sub>2</sub> CHO	84.54240	4 <sub>0,4,5</sub> → 3 <sub>0,3,4</sub>	-3.9935	10.1572	1.12 ± 0.17	0.012 ± 0.007
NH <sub>2</sub> CHO	84.54240	4 <sub>0,4,4</sub> → 3 <sub>0,3,3</sub>	-4.1087	10.1572	0.86 ± 0.17	(10 ± 6) · 10 <sup>-3</sup>
NH <sub>2</sub> CHO	84.54240	4 <sub>0,4,3</sub> → 3 <sub>0,3,2</sub>	-4.2268	10.1572	0.66 ± 0.17	(7 ± 6) · 10 <sup>-3</sup>
NH <sub>2</sub> CHO	84.54312	4 <sub>0,4,4</sub> → 3 <sub>0,3,4</sub>	-5.2848	10.1572	0.06 ± 0.17	(1 ± 6) · 10 <sup>-3</sup>
NH <sub>2</sub> CHO	85.09324	4 <sub>2,2,3</sub> → 3 <sub>2,1,2</sub>	-4.3631	22.120	0.24 ± 0.17	(3 ± 6) · 10 <sup>-3</sup>
NH <sub>2</sub> CHO	85.09330	4 <sub>2,2,5</sub> → 3 <sub>2,1,4</sub>	-4.1298	22.120	0.41 ± 0.17	(5 ± 6) · 10 <sup>-3</sup>
NH <sub>2</sub> CHO	85.09332	4 <sub>2,2,3</sub> → 3 <sub>2,1,3</sub>	-5.4211	22.120	0.02 ± 0.17	(0 ± 6) · 10 <sup>-3</sup>
NH <sub>2</sub> CHO	85.09347	4 <sub>2,2,4</sub> → 3 <sub>2,1,4</sub>	-5.4211	22.120	0.02 ± 0.17	(0 ± 6) · 10 <sup>-3</sup>

Table S 1: Continued.

Molecule	Frequency (GHz)	Transition	$\log I$ ( $\text{nm}^2 \text{ MHz}$ )	$E_{\text{up}}$ (K)	Area ( $\text{K km s}^{-1}$ )	$\tau$
NH <sub>2</sub> CHO	85.09353	4 <sub>2,2,4</sub> → 3 <sub>2,1,3</sub>	−4.2450	22.120	0.31 ± 0.17	(3 ± 6) · 10 <sup>−3</sup>
NH <sub>2</sub> CHO	87.84853	4 <sub>1,3,4</sub> → 3 <sub>1,2,4</sub>	−5.2840	13.5244	0.05 ± 0.17	(1 ± 6) · 10 <sup>−3</sup>
NH <sub>2</sub> CHO	87.84886	4 <sub>1,3,3</sub> → 3 <sub>1,2,2</sub>	−4.2260	13.5244	0.52 ± 0.17	(6 ± 6) · 10 <sup>−3</sup>
NH <sub>2</sub> CHO	87.84891	4 <sub>1,3,5</sub> → 3 <sub>1,2,4</sub>	−3.9928	13.5245	0.89 ± 0.17	(10 ± 6) · 10 <sup>−3</sup>
NH <sub>2</sub> CHO	87.84898	4 <sub>1,3,4</sub> → 3 <sub>1,2,3</sub>	−4.1079	13.5245	0.68 ± 0.17	(8 ± 6) · 10 <sup>−3</sup>
NH <sub>2</sub> CHO	87.84946	4 <sub>1,3,3</sub> → 3 <sub>1,2,3</sub>	−5.2840	13.5245	0.05 ± 0.17	(1 ± 6) · 10 <sup>−3</sup>
NH <sub>2</sub> CHO	102.06241	5 <sub>1,5,4</sub> → 4 <sub>1,4,4</sub>	−5.2459	17.6839	0.03 ± 0.17	(0 ± 6) · 10 <sup>−3</sup>
NH <sub>2</sub> CHO	102.06431	5 <sub>1,5,6</sub> → 4 <sub>1,4,5</sub>	−3.7754	17.6840	1.00 ± 0.17	0.011 ± 0.007
NH <sub>2</sub> CHO	102.06438	5 <sub>1,5,4</sub> → 4 <sub>1,4,3</sub>	−3.9571	17.6840	0.66 ± 0.17	(7 ± 6) · 10 <sup>−3</sup>
NH <sub>2</sub> CHO	102.06438	5 <sub>1,5,5</sub> → 4 <sub>1,4,4</sub>	−3.8657	17.6840	0.82 ± 0.17	(9 ± 6) · 10 <sup>−3</sup>
NH <sub>2</sub> CHO	102.06595	5 <sub>1,5,5</sub> → 4 <sub>1,4,5</sub>	−5.2459	17.6841	0.03 ± 0.17	(0 ± 6) · 10 <sup>−3</sup>
NH <sub>2</sub> CHO	105.46330	5 <sub>0,5,4</sub> → 4 <sub>0,4,4</sub>	−5.1964	15.2187	0.04 ± 0.17	(0 ± 6) · 10 <sup>−3</sup>
NH <sub>2</sub> CHO	105.46426	5 <sub>0,5,6</sub> → 4 <sub>0,4,5</sub>	−3.7259	15.2187	1.26 ± 0.17	0.014 ± 0.007
NH <sub>2</sub> CHO	105.46429	5 <sub>0,5,4</sub> → 4 <sub>0,4,3</sub>	−3.9076	15.2187	0.83 ± 0.17	(9 ± 7) · 10 <sup>−3</sup>
NH <sub>2</sub> CHO	105.46433	5 <sub>0,5,5</sub> → 4 <sub>0,4,4</sub>	−3.8162	15.2187	1.02 ± 0.17	0.012 ± 0.007
NH <sub>2</sub> CHO	105.46511	5 <sub>0,5,5</sub> → 4 <sub>0,4,5</sub>	−5.1964	15.2188	0.04 ± 0.17	(0 ± 6) · 10 <sup>−3</sup>
NH <sub>2</sub> CHO	105.97232	5 <sub>2,4,4</sub> → 4 <sub>2,3,4</sub>	−5.2848	27.185	0.02 ± 0.17	(0 ± 6) · 10 <sup>−3</sup>
NH <sub>2</sub> CHO	105.97266	5 <sub>2,4,4</sub> → 4 <sub>2,3,3</sub>	−3.9961	27.185	0.34 ± 0.17	(4 ± 6) · 10 <sup>−3</sup>
NH <sub>2</sub> CHO	105.97268	5 <sub>2,4,6</sub> → 4 <sub>2,3,5</sub>	−3.8144	27.185	0.51 ± 0.17	(6 ± 6) · 10 <sup>−3</sup>
NH <sub>2</sub> CHO	105.97283	5 <sub>2,4,5</sub> → 4 <sub>2,3,4</sub>	−3.9046	27.185	0.41 ± 0.17	(5 ± 6) · 10 <sup>−3</sup>
NH <sub>2</sub> CHO	105.97311	5 <sub>2,4,5</sub> → 4 <sub>2,3,5</sub>	−5.2848	27.185	0.02 ± 0.17	(0 ± 6) · 10 <sup>−3</sup>
NH <sub>2</sub> CHO	106.54156	5 <sub>2,3,4</sub> → 4 <sub>2,2,4</sub>	−5.2802	27.233	0.02 ± 0.17	(0 ± 6) · 10 <sup>−3</sup>
NH <sub>2</sub> CHO	106.54177	5 <sub>2,3,4</sub> → 4 <sub>2,2,3</sub>	−3.9914	27.233	0.34 ± 0.17	(4 ± 6) · 10 <sup>−3</sup>
NH <sub>2</sub> CHO	106.54178	5 <sub>2,3,6</sub> → 4 <sub>2,2,5</sub>	−3.8098	27.233	0.51 ± 0.17	(6 ± 6) · 10 <sup>−3</sup>
NH <sub>2</sub> CHO	106.54187	5 <sub>2,3,5</sub> → 4 <sub>2,2,4</sub>	−3.9000	27.233	0.41 ± 0.17	(5 ± 6) · 10 <sup>−3</sup>
NH <sub>2</sub> CHO	106.54204	5 <sub>2,3,5</sub> → 4 <sub>2,2,5</sub>	−5.2802	27.233	0.02 ± 0.17	(0 ± 6) · 10 <sup>−3</sup>
NH <sub>2</sub> CHO	109.75324	5 <sub>1,4,5</sub> → 4 <sub>1,3,5</sub>	−5.1842	18.7917	0.03 ± 0.17	(0 ± 6) · 10 <sup>−3</sup>
NH <sub>2</sub> CHO	109.75355	5 <sub>1,4,4</sub> → 4 <sub>1,3,3</sub>	−3.8954	18.7917	0.67 ± 0.17	(8 ± 6) · 10 <sup>−3</sup>
NH <sub>2</sub> CHO	109.75358	5 <sub>1,4,6</sub> → 4 <sub>1,3,5</sub>	−3.7137	18.7917	1.01 ± 0.17	0.011 ± 0.007
NH <sub>2</sub> CHO	109.75362	5 <sub>1,4,5</sub> → 4 <sub>1,3,4</sub>	−3.8039	18.7917	0.82 ± 0.17	(9 ± 7) · 10 <sup>−3</sup>
NH <sub>2</sub> CHO	109.75403	5 <sub>1,4,4</sub> → 4 <sub>1,3,4</sub>	−5.1842	18.7917	0.03 ± 0.17	(0 ± 6) · 10 <sup>−3</sup>
HCS <sup>+</sup>	85.34789	2 → 1	−2.9031	6.1441	4.17 ± 0.16	0.061 ± 0.006
H <sub>2</sub> CS	101.47762	3 <sub>1,3</sub> → 2 <sub>1,2</sub>	−3.6341	22.930	6.57 ± 0.17	0.097 ± 0.018
H <sub>2</sub> CS	101.47762	3 <sub>1,3</sub> → 2 <sub>1,2</sub>	−3.6341	22.930	18.2 ± 0.3	0.021 ± 0.010
H <sub>2</sub> CS	103.03999	3 <sub>2,2</sub> → 2 <sub>2,1</sub>	−4.3594	62.592	0.27 ± 0.17	(4 ± 6) · 10 <sup>−3</sup>
H <sub>2</sub> CS	103.03999	3 <sub>2,2</sub> → 2 <sub>2,1</sub>	−4.3594	62.592	2.5 ± 0.3	(2.9 ± 1.9) · 10 <sup>−3</sup>
H <sub>2</sub> CS	103.04022	3 <sub>0,3</sub> → 2 <sub>0,2</sub>	−4.0278	9.8908	4.36 ± 0.17	0.064 ± 0.013
H <sub>2</sub> CS	103.04022	3 <sub>0,3</sub> → 2 <sub>0,2</sub>	−4.0278	9.8908	8.1 ± 0.3	(9 ± 5) · 10 <sup>−3</sup>
H <sub>2</sub> CS	103.05181	3 <sub>2,1</sub> → 2 <sub>2,0</sub>	−4.3593	62.593	0.27 ± 0.17	(4 ± 6) · 10 <sup>−3</sup>
H <sub>2</sub> CS	103.05181	3 <sub>2,1</sub> → 2 <sub>2,0</sub>	−4.3593	62.593	2.5 ± 0.3	(2.9 ± 1.9) · 10 <sup>−3</sup>
H <sub>2</sub> CS	104.61704	3 <sub>1,2</sub> → 2 <sub>1,1</sub>	−3.6079	23.231	6.69 ± 0.17	0.099 ± 0.019
H <sub>2</sub> CS	104.61704	3 <sub>1,2</sub> → 2 <sub>1,1</sub>	−3.6079	23.231	18.7 ± 0.3	0.022 ± 0.011
CH <sub>3</sub> OCH <sub>3</sub>	90.93751	6 <sub>0,6,0</sub> → 5 <sub>1,5,0</sub>	−5.7994	18.9745	0.27 ± 0.12	(2 ± 3) · 10 <sup>−3</sup>
CH <sub>3</sub> OCH <sub>3</sub>	90.93811	6 <sub>0,6,1</sub> → 5 <sub>1,5,1</sub>	−5.3735	18.9758	0.73 ± 0.12	(6 ± 3) · 10 <sup>−3</sup>
CH <sub>3</sub> OCH <sub>3</sub>	90.93870	6 <sub>0,6,5</sub> → 5 <sub>1,5,5</sub>	−6.2764	18.9759	0.09 ± 0.12	(1 ± 3) · 10 <sup>−3</sup>
CH <sub>3</sub> OCH <sub>3</sub>	90.93871	6 <sub>0,6,3</sub> → 5 <sub>1,5,3</sub>	−5.9756	18.9759	0.18 ± 0.12	(1 ± 3) · 10 <sup>−3</sup>
CH <sub>3</sub> OCH <sub>3</sub>	93.85444	4 <sub>2,3,3</sub> → 4 <sub>1,4,3</sub>	−6.1525	14.7172	0.14 ± 0.12	(1 ± 3) · 10 <sup>−3</sup>
CH <sub>3</sub> OCH <sub>3</sub>	93.85456	4 <sub>2,3,5</sub> → 4 <sub>1,4,5</sub>	−5.9763	14.7171	0.21 ± 0.12	(2 ± 3) · 10 <sup>−3</sup>
CH <sub>3</sub> OCH <sub>3</sub>	93.85711	4 <sub>2,3,1</sub> → 4 <sub>1,4,1</sub>	−5.5504	14.7172	0.56 ± 0.12	(4 ± 3) · 10 <sup>−3</sup>
CH <sub>3</sub> OCH <sub>3</sub>	93.85973	4 <sub>2,3,0</sub> → 4 <sub>1,4,0</sub>	−5.7544	14.7172	0.35 ± 0.12	(3 ± 3) · 10 <sup>−3</sup>
CH <sub>3</sub> OCH <sub>3</sub>	96.84724	5 <sub>2,4,3</sub> → 5 <sub>1,5,3</sub>	−6.0392	19.2593	0.15 ± 0.12	(1 ± 3) · 10 <sup>−3</sup>
CH <sub>3</sub> OCH <sub>3</sub>	96.84729	5 <sub>2,4,5</sub> → 5 <sub>1,5,5</sub>	−6.3404	19.2593	0.07 ± 0.12	(1 ± 3) · 10 <sup>−3</sup>
CH <sub>3</sub> OCH <sub>3</sub>	96.84989	5 <sub>2,4,1</sub> → 5 <sub>1,5,1</sub>	−5.4372	19.2593	0.59 ± 0.12	(4 ± 3) · 10 <sup>−3</sup>
CH <sub>3</sub> OCH <sub>3</sub>	96.85251	5 <sub>2,4,0</sub> → 5 <sub>1,5,0</sub>	−5.8631	19.2593	0.22 ± 0.12	(2 ± 3) · 10 <sup>−3</sup>
CH <sub>3</sub> OCH <sub>3</sub>	99.32436	4 <sub>1,4,3</sub> → 3 <sub>0,3,3</sub>	−5.9773	10.2138	0.24 ± 0.12	(2 ± 3) · 10 <sup>−3</sup>
CH <sub>3</sub> OCH <sub>3</sub>	99.32436	4 <sub>1,4,5</sub> → 3 <sub>0,3,5</sub>	−5.8012	10.2138	0.36 ± 0.12	(3 ± 3) · 10 <sup>−3</sup>
CH <sub>3</sub> OCH <sub>3</sub>	99.32522	4 <sub>1,4,1</sub> → 3 <sub>0,3,1</sub>	−5.3752	10.2124	0.96 ± 0.12	(7 ± 4) · 10 <sup>−3</sup>

Table S 1: Continued.

Molecule	Frequency (GHz)	Transition	$\log I$ (nm <sup>2</sup> MHz)	$E_{\text{up}}$ (K)	Area (K km s <sup>-1</sup> )	$\tau$
CH <sub>3</sub> OCH <sub>3</sub>	99.32607	4 <sub>1,4,0</sub> → 3 <sub>0,3,0</sub>	-5.5793	10.2123	0.60 ± 0.12	(5 ± 3) · 10 <sup>-3</sup>
CH <sub>3</sub> OCH <sub>3</sub>	111.78225	7 <sub>4,4,3</sub> → 8 <sub>5,3,3</sub>	-8.5795	60.631	0.00 ± 0.12	(0 ± 3) · 10 <sup>-3</sup>
CH <sub>3</sub> OCH <sub>3</sub>	111.78260	7 <sub>0,7,0</sub> → 6 <sub>1,6,0</sub>	-5.3051	25.249	0.54 ± 0.12	(4 ± 3) · 10 <sup>-3</sup>
CH <sub>3</sub> OCH <sub>3</sub>	111.78312	7 <sub>0,7,1</sub> → 6 <sub>1,6,1</sub>	-5.1010	25.249	0.87 ± 0.12	(7 ± 3) · 10 <sup>-3</sup>
CH <sub>3</sub> OCH <sub>3</sub>	111.78363	7 <sub>0,7,5</sub> → 6 <sub>1,6,5</sub>	-5.5269	25.250	0.32 ± 0.12	(2 ± 3) · 10 <sup>-3</sup>
CH <sub>3</sub> OCH <sub>3</sub>	111.78363	7 <sub>0,7,3</sub> → 6 <sub>1,6,3</sub>	-5.7030	25.250	0.22 ± 0.12	(2 ± 3) · 10 <sup>-3</sup>
CH <sub>3</sub> OCH <sub>3</sub>	115.54399	5 <sub>1,5,3</sub> → 4 <sub>0,4,3</sub>	-5.7603	14.6122	0.29 ± 0.12	(2 ± 3) · 10 <sup>-3</sup>
CH <sub>3</sub> OCH <sub>3</sub>	115.54400	5 <sub>1,5,5</sub> → 4 <sub>0,4,5</sub>	-6.0613	14.6122	0.14 ± 0.12	(1 ± 3) · 10 <sup>-3</sup>
CH <sub>3</sub> OCH <sub>3</sub>	115.54481	5 <sub>1,5,1</sub> → 4 <sub>0,4,1</sub>	-5.1583	14.6106	1.14 ± 0.12	(9 ± 4) · 10 <sup>-3</sup>
CH <sub>3</sub> OCH <sub>3</sub>	115.54562	5 <sub>1,5,0</sub> → 4 <sub>0,4,0</sub>	-5.5843	14.6107	0.43 ± 0.12	(3 ± 3) · 10 <sup>-3</sup>
NS	115.15394	3 <sub>1,3,4</sub> → 2 <sub>-1,2,3</sub>	-3.3836	8.8381	9.3 ± 0.2	0.096 ± 0.007
NS	115.15681	3 <sub>1,3,3</sub> → 2 <sub>-1,2,2</sub>	-3.5843	8.8398	5.9 ± 0.2	0.060 ± 0.007
NS	115.16298	3 <sub>1,3,2</sub> → 2 <sub>-1,2,1</sub>	-3.8096	8.8413	3.6 ± 0.2	0.036 ± 0.006
NS	115.18534	3 <sub>1,3,2</sub> → 2 <sub>-1,2,2</sub>	-4.3045	8.8412	1.1 ± 0.2	0.011 ± 0.006
NS	115.19146	3 <sub>1,3,3</sub> → 2 <sub>-1,2,3</sub>	-4.3045	8.8399	1.1 ± 0.2	0.011 ± 0.006
NS	115.48941	3 <sub>-1,3,3</sub> → 2 <sub>1,2,3</sub>	-4.3015	8.8957	1.2 ± 0.2	0.011 ± 0.006
NS	115.52460	3 <sub>-1,3,2</sub> → 2 <sub>1,2,2</sub>	-4.3015	8.8935	1.2 ± 0.2	0.011 ± 0.006
NS	115.55625	3 <sub>-1,3,4</sub> → 2 <sub>1,2,3</sub>	-3.3807	8.8989	9.3 ± 0.2	0.096 ± 0.007
NS	115.57076	3 <sub>-1,3,3</sub> → 2 <sub>1,2,2</sub>	-3.5814	8.8957	5.9 ± 0.2	0.060 ± 0.007
NS	115.57195	3 <sub>-1,3,2</sub> → 2 <sub>1,2,1</sub>	-3.8067	8.8934	3.6 ± 0.2	0.036 ± 0.006
C <sub>2</sub> H <sub>5</sub> OH	85.26549	6 <sub>0,6,2</sub> → 5 <sub>1,5,2</sub>	-5.1507	17.4834	1.23 ± 0.12	(6 ± 3) · 10 <sup>-3</sup>
C <sub>2</sub> H <sub>5</sub> OH	87.71612	5 <sub>2,4,2</sub> → 5 <sub>1,5,2</sub>	-5.2625	17.6010	0.92 ± 0.12	(5 ± 2) · 10 <sup>-3</sup>
C <sub>2</sub> H <sub>5</sub> OH	90.11760	4 <sub>1,4,2</sub> → 3 <sub>0,3,2</sub>	-5.1938	9.3498	1.46 ± 0.12	(7 ± 3) · 10 <sup>-3</sup>
C <sub>2</sub> H <sub>5</sub> OH	91.48519	6 <sub>2,5,2</sub> → 6 <sub>1,6,2</sub>	-5.1662	22.627	0.90 ± 0.12	(4 ± 2) · 10 <sup>-3</sup>
C <sub>2</sub> H <sub>5</sub> OH	100.99011	8 <sub>2,7,2</sub> → 8 <sub>1,8,2</sub>	-5.0075	35.173	0.72 ± 0.12	(4 ± 2) · 10 <sup>-3</sup>
C <sub>2</sub> H <sub>5</sub> OH	103.70288	9 <sub>1,8,2</sub> → 8 <sub>2,7,2</sub>	-5.1715	40.150	0.39 ± 0.12	(2 ± 2) · 10 <sup>-3</sup>
C <sub>2</sub> H <sub>5</sub> OH	104.48724	7 <sub>0,7,2</sub> → 6 <sub>1,6,2</sub>	-4.8788	23.251	1.50 ± 0.12	(7 ± 3) · 10 <sup>-3</sup>
C <sub>2</sub> H <sub>5</sub> OH	104.80862	5 <sub>1,5,2</sub> → 4 <sub>0,4,2</sub>	-4.9749	13.3914	1.78 ± 0.12	(9 ± 3) · 10 <sup>-3</sup>
C <sub>2</sub> H <sub>5</sub> OH	106.72356	9 <sub>2,8,2</sub> → 9 <sub>1,9,2</sub>	-4.9393	42.688	0.59 ± 0.12	(3 ± 2) · 10 <sup>-3</sup>
C <sub>2</sub> H <sub>5</sub> OH	112.80719	2 <sub>2,1,2</sub> → 1 <sub>1,0,2</sub>	-5.2320	7.5372	1.16 ± 0.12	(6 ± 3) · 10 <sup>-3</sup>
C <sub>2</sub> H <sub>5</sub> OH	114.06494	2 <sub>2,0,2</sub> → 1 <sub>1,1,2</sub>	-5.2326	7.5392	1.15 ± 0.12	(6 ± 3) · 10 <sup>-3</sup>
CH <sub>3</sub> SH	100.11022	4 <sub>1,3,0</sub> → 3 <sub>1,2,0</sub>	-4.7606	17.0863	1.00 ± 0.11	0.019 ± 0.010
CH <sub>3</sub> SH	101.02974	4 <sub>-1,4,1</sub> → 3 <sub>-1,3,1</sub>	-4.7524	16.6895	1.04 ± 0.11	0.020 ± 0.010
CH <sub>3</sub> SH	101.13915	4 <sub>0,4,0</sub> → 3 <sub>0,3,0</sub>	-4.7166	12.1359	1.65 ± 0.11	0.032 ± 0.013
CH <sub>3</sub> SH	101.13965	4 <sub>0,4,1</sub> → 3 <sub>0,3,1</sub>	-4.7183	13.5618	1.46 ± 0.11	0.029 ± 0.012
CH <sub>3</sub> SH	101.28437	4 <sub>1,3,1</sub> → 3 <sub>1,2,1</sub>	-4.7525	18.3326	0.91 ± 0.11	0.018 ± 0.009
CH <sub>3</sub> SH	102.20247	4 <sub>-1,4,0</sub> → 3 <sub>-1,3,0</sub>	-4.7429	17.3373	1.00 ± 0.11	0.020 ± 0.010
HC <sub>3</sub> N	90.97902	10 → 9	-2.2848	24.015	51.9 ± 0.4	0.23 ± 0.02
HC <sub>3</sub> N	90.97902	10 → 9	-2.2848	24.015	11.0 ± 0.2	0.14 ± 0.03
HC <sub>3</sub> N	100.07639	11 → 10	-2.1673	28.818	52.2 ± 0.4	0.23 ± 0.02
HC <sub>3</sub> N	100.07639	11 → 10	-2.1673	28.818	11.4 ± 0.2	0.15 ± 0.03
HC <sub>3</sub> N	109.17363	12 → 11	-2.0612	34.057	50.9 ± 0.4	0.23 ± 0.02
HC <sub>3</sub> N	109.17363	12 → 11	-2.0612	34.057	11.4 ± 0.2	0.15 ± 0.03
H <sup>13</sup> CCCN	88.16683	10 → 9	-2.3247	23.272	0.86 ± 0.12	0.011 ± 0.004
H <sup>13</sup> CCCN	96.98300	11 → 10	-2.2070	27.927	0.83 ± 0.12	0.010 ± 0.004
H <sup>13</sup> CCCN	105.79911	12 → 11	-2.1007	33.004	0.77 ± 0.12	(10 ± 4) · 10 <sup>-3</sup>
H <sup>13</sup> CCCN	114.61499	13 → 12	-2.0040	38.505	0.69 ± 0.12	(9 ± 4) · 10 <sup>-3</sup>
HC <sup>13</sup> CCN	90.59306	10 → 9	-2.2902	23.913	0.86 ± 0.11	0.011 ± 0.004
HC <sup>13</sup> CCN	99.65185	11 → 10	-2.1726	28.695	0.82 ± 0.11	0.010 ± 0.004
HC <sup>13</sup> CCN	108.71053	12 → 11	-2.0665	33.913	0.76 ± 0.11	(10 ± 4) · 10 <sup>-3</sup>
HCC <sup>13</sup> CN	90.60178	10 → 9	-2.2901	23.915	1.01 ± 0.14	0.011 ± 0.011
HCC <sup>13</sup> CN	99.66147	11 → 10	-2.1725	28.698	0.99 ± 0.14	0.011 ± 0.011
HCC <sup>13</sup> CN	108.72100	12 → 11	-2.0664	33.916	0.93 ± 0.14	0.011 ± 0.010
C <sub>2</sub> H <sub>3</sub> CN	84.94600	9 <sub>0,9</sub> → 8 <sub>0,8</sub>	-3.9103	20.429	1.41 ± 0.13	0.031 ± 0.011
C <sub>2</sub> H <sub>3</sub> CN	85.30264	9 <sub>2,8</sub> → 8 <sub>2,7</sub>	-3.9411	29.135	0.56 ± 0.13	0.012 ± 0.009
C <sub>2</sub> H <sub>3</sub> CN	87.31281	9 <sub>1,8</sub> → 8 <sub>1,7</sub>	-3.8955	23.129	1.09 ± 0.13	0.024 ± 0.010
C <sub>2</sub> H <sub>3</sub> CN	92.42625	10 <sub>1,10</sub> → 9 <sub>1,9</sub>	-3.8041	26.578	0.91 ± 0.13	0.020 ± 0.010
C <sub>2</sub> H <sub>3</sub> CN	94.27664	10 <sub>0,10</sub> → 9 <sub>0,9</sub>	-3.7803	24.953	1.11 ± 0.13	0.024 ± 0.010



Table S 1: Continued.

Molecule	Frequency (GHz)	Transition	$\log I$ (nm <sup>2</sup> MHz)	$E_{\text{up}}$ (K)	Area (K km s <sup>-1</sup> )	$\tau$
C <sub>2</sub> H <sub>3</sub> CN	94.76078	10 <sub>2,9</sub> → 9 <sub>2,8</sub>	-3.8060	33.682	0.44 ± 0.13	(10 ± 9) · 10 <sup>-3</sup>
C <sub>2</sub> H <sub>3</sub> CN	95.32548	10 <sub>2,8</sub> → 9 <sub>2,7</sub>	-3.8009	33.764	0.44 ± 0.13	(10 ± 9) · 10 <sup>-3</sup>
C <sub>2</sub> H <sub>3</sub> CN	96.98244	10 <sub>1,9</sub> → 9 <sub>1,8</sub>	-3.7639	27.783	0.85 ± 0.13	0.019 ± 0.010
C <sub>2</sub> H <sub>3</sub> CN	101.63723	11 <sub>1,11</sub> → 10 <sub>1,10</sub>	-3.6862	31.456	0.68 ± 0.13	0.015 ± 0.010
C <sub>2</sub> H <sub>3</sub> CN	103.57540	11 <sub>0,11</sub> → 10 <sub>0,10</sub>	-3.6642	29.924	0.82 ± 0.13	0.018 ± 0.010
C <sub>2</sub> H <sub>3</sub> CN	104.21265	11 <sub>2,10</sub> → 10 <sub>2,9</sub>	-3.6858	38.684	0.33 ± 0.13	(7 ± 9) · 10 <sup>-3</sup>
C <sub>2</sub> H <sub>3</sub> CN	104.96054	11 <sub>2,9</sub> → 10 <sub>2,8</sub>	-3.6797	38.801	0.33 ± 0.13	(7 ± 9) · 10 <sup>-3</sup>
C <sub>2</sub> H <sub>3</sub> CN	106.64139	11 <sub>1,10</sub> → 10 <sub>1,9</sub>	-3.6464	32.901	0.62 ± 0.13	0.014 ± 0.010
C <sub>2</sub> H <sub>3</sub> CN	110.83998	12 <sub>1,12</sub> → 11 <sub>1,11</sub>	-3.5799	36.775	0.48 ± 0.13	0.011 ± 0.010
C <sub>2</sub> H <sub>3</sub> CN	112.84064	12 <sub>0,12</sub> → 11 <sub>0,11</sub>	-3.5595	35.339	0.57 ± 0.13	0.013 ± 0.010
CH <sub>3</sub> OCHO	88.84319	7 <sub>1,6,2</sub> → 6 <sub>1,5,2</sub>	-5.0452	17.9569	0.37 ± 0.08	(3 ± 2) · 10 <sup>-3</sup>
CH <sub>3</sub> OCHO	88.85161	7 <sub>1,6,0</sub> → 6 <sub>1,5,0</sub>	-5.0450	17.9395	0.37 ± 0.08	(3 ± 2) · 10 <sup>-3</sup>
CH <sub>3</sub> OCHO	90.14572	7 <sub>2,5,2</sub> → 6 <sub>2,4,2</sub>	-5.0573	19.6834	0.34 ± 0.08	(2 ± 2) · 10 <sup>-3</sup>
CH <sub>3</sub> OCHO	90.15647	7 <sub>2,5,0</sub> → 6 <sub>2,4,0</sub>	-5.0570	19.6666	0.34 ± 0.08	(2 ± 2) · 10 <sup>-3</sup>
CH <sub>3</sub> OCHO	90.22766	8 <sub>0,8,2</sub> → 7 <sub>0,7,2</sub>	-4.9710	20.080	0.41 ± 0.08	(3 ± 2) · 10 <sup>-3</sup>
CH <sub>3</sub> OCHO	90.22962	8 <sub>0,8,0</sub> → 7 <sub>0,7,0</sub>	-4.9708	20.061	0.41 ± 0.08	(3 ± 2) · 10 <sup>-3</sup>
CH <sub>3</sub> OCHO	96.07073	8 <sub>2,7,1</sub> → 7 <sub>2,6,1</sub>	-4.9438	23.609	0.36 ± 0.08	(2 ± 2) · 10 <sup>-3</sup>
CH <sub>3</sub> OCHO	96.07685	8 <sub>2,7,0</sub> → 7 <sub>2,6,0</sub>	-4.9436	23.592	0.36 ± 0.08	(2 ± 2) · 10 <sup>-3</sup>
CH <sub>3</sub> OCHO	98.60686	8 <sub>3,6,1</sub> → 7 <sub>3,5,1</sub>	-4.9628	27.260	0.29 ± 0.08	(2 ± 2) · 10 <sup>-3</sup>
CH <sub>3</sub> OCHO	98.61116	8 <sub>3,6,0</sub> → 7 <sub>3,5,0</sub>	-4.9621	27.244	0.29 ± 0.08	(2 ± 2) · 10 <sup>-3</sup>
CH <sub>3</sub> OCHO	100.68154	9 <sub>0,9,2</sub> → 8 <sub>0,8,2</sub>	-4.8307	24.912	0.42 ± 0.08	(3 ± 2) · 10 <sup>-3</sup>
CH <sub>3</sub> OCHO	100.68337	9 <sub>0,9,0</sub> → 8 <sub>0,8,0</sub>	-4.8306	24.893	0.42 ± 0.08	(3 ± 2) · 10 <sup>-3</sup>
CH <sub>3</sub> OCHO	103.46657	8 <sub>2,6,2</sub> → 7 <sub>2,5,2</sub>	-4.8771	24.649	0.37 ± 0.08	(3 ± 2) · 10 <sup>-3</sup>
CH <sub>3</sub> OCHO	103.47866	8 <sub>2,6,0</sub> → 7 <sub>2,5,0</sub>	-4.8769	24.633	0.38 ± 0.08	(3 ± 2) · 10 <sup>-3</sup>
CH <sub>3</sub> OCHO	110.78866	10 <sub>1,10,1</sub> → 9 <sub>1,9,1</sub>	-4.7090	30.274	0.42 ± 0.08	(3 ± 2) · 10 <sup>-3</sup>
CH <sub>3</sub> OCHO	110.79053	10 <sub>1,10,0</sub> → 9 <sub>1,9,0</sub>	-4.7088	30.256	0.42 ± 0.08	(3 ± 2) · 10 <sup>-3</sup>
CH <sub>3</sub> OCHO	111.16990	10 <sub>0,10,2</sub> → 9 <sub>0,9,2</sub>	-4.7056	30.247	0.42 ± 0.08	(3 ± 2) · 10 <sup>-3</sup>
CH <sub>3</sub> OCHO	111.17163	10 <sub>0,10,0</sub> → 9 <sub>0,9,0</sub>	-4.7055	30.229	0.43 ± 0.08	(3 ± 2) · 10 <sup>-3</sup>
CH <sub>3</sub> OCHO	111.22349	9 <sub>4,6,1</sub> → 8 <sub>4,5,1</sub>	-4.8737	37.234	0.22 ± 0.08	(1.5 ± 1.9) · 10 <sup>-3</sup>
OCS	85.13910	7 → 6	-3.7954	16.3442	8.72 ± 0.19	0.119 ± 0.007
OCS	85.13910	7 → 6	-3.7954	16.3442	10.5 ± 0.3	0.037 ± 0.009
OCS	97.30121	8 → 7	-3.6277	21.014	9.07 ± 0.19	0.125 ± 0.008
OCS	97.30121	8 → 7	-3.6277	21.014	11.8 ± 0.3	0.042 ± 0.010
OCS	109.46306	9 → 8	-3.4815	26.267	8.90 ± 0.19	0.123 ± 0.008
OCS	109.46306	9 → 8	-3.4815	26.267	12.6 ± 0.3	0.044 ± 0.011
HC <sub>5</sub> N	85.20134	32 → 31	-2.3041	67.470	0.85 ± 0.09	(5 ± 2) · 10 <sup>-3</sup>
HC <sub>5</sub> N	87.86363	33 → 32	-2.2700	71.686	0.81 ± 0.09	(5 ± 2) · 10 <sup>-3</sup>
HC <sub>5</sub> N	90.52589	34 → 33	-2.2373	76.031	0.77 ± 0.09	(5 ± 2) · 10 <sup>-3</sup>
HC <sub>5</sub> N	93.18812	35 → 34	-2.2059	80.503	0.73 ± 0.09	(4 ± 2) · 10 <sup>-3</sup>
HC <sub>5</sub> N	95.85034	36 → 35	-2.1758	85.103	0.68 ± 0.09	(4 ± 2) · 10 <sup>-3</sup>
HC <sub>5</sub> N	98.51252	37 → 36	-2.1469	89.831	0.64 ± 0.09	(3.9 ± 1.9) · 10 <sup>-3</sup>
HC <sub>5</sub> N	101.17468	38 → 37	-2.1190	94.687	0.59 ± 0.09	(3.7 ± 1.9) · 10 <sup>-3</sup>
HC <sub>5</sub> N	103.83682	39 → 38	-2.0923	99.670	0.55 ± 0.09	(3.4 ± 1.8) · 10 <sup>-3</sup>
Non detected molecules						
HC <sup>17</sup> O <sup>+</sup>	87.05753	1 → 0	-2.2763	4.2	0.27	1.42 · 10 <sup>-3</sup>
CH <sub>3</sub> NH <sub>2</sub>	95.14532	4 <sub>0,4</sub> → 3 <sub>1,-4</sub>	-4.9066	22	0.32	2.7 · 10 <sup>-3</sup>
CH <sub>3</sub> NC	100.52425	5 <sub>1</sub> → 4 <sub>1</sub>	-3.0053	22	0.140	1.22 · 10 <sup>-3</sup>
CH <sub>3</sub> NC	100.52654	5 <sub>0</sub> → 4 <sub>0</sub>	-2.9773	14.5	0.21	1.80 · 10 <sup>-3</sup>
HOCN	104.87468	5 <sub>0,5</sub> → 4 <sub>0,4</sub>	-2.8221	15.1	0.43	3.7 · 10 <sup>-3</sup>
c-C <sub>2</sub> H <sub>4</sub> O	94.66454	3 <sub>1,3</sub> → 2 <sub>0,2</sub>	-4.1955	9.5	0.29	2.5 · 10 <sup>-3</sup>
t-HCOOH	111.74678	5 <sub>0,5</sub> → 4 <sub>0,4</sub>	-4.0451	16.1	0.31	2.7 · 10 <sup>-3</sup>
HONO	93.95279	4 <sub>0,4,0</sub> → 3 <sub>0,3,0</sub>	-4.4413	11.3	0.44	3.8 · 10 <sup>-3</sup>
Z-HNCHCN	86.99658	9 <sub>0,9</sub> → 8 <sub>0,8</sub>	-4.5025	21	0.39	3.3 · 10 <sup>-3</sup>
C <sub>2</sub> H <sub>5</sub> CN	88.32373	10 <sub>0,10</sub> → 9 <sub>0,9</sub>	-3.7186	23	0.174	1.50 × 10 <sup>-3</sup>
CH <sub>3</sub> NCO	86.68019	10 <sub>0,10,0</sub> → 9 <sub>0,9,0</sub>	-4.5525	23	0.111	7.9 × 10 <sup>-4</sup>
C <sub>2</sub> H <sub>5</sub> CHO	87.02285	9 <sub>0,9,0</sub> → 8 <sub>0,8,0</sub>	-4.8295	21	0.146	1.26 × 10 <sup>-3</sup>
C <sub>2</sub> H <sub>5</sub> CHO	87.02285	9 <sub>0,9,1</sub> → 8 <sub>0,8,1</sub>	-4.8295	21	0.146	1.26 × 10 <sup>-3</sup>

Table S 1: Continued.

Molecule	Frequency (GHz)	Transition	$\log I$ (nm <sup>2</sup> MHz)	$E_{\text{up}}$ (K)	Area (K km s <sup>-1</sup> )	$\tau$
CH <sub>3</sub> COCH <sub>3</sub>	92.73567	9 <sub>0,9,0</sub> → 8 <sub>1,8,1</sub>	-5.4014	23	0.112	$8.0 \times 10^{-4}$
CH <sub>3</sub> COCH <sub>3</sub>	92.73567	9 <sub>1,9,0</sub> → 8 <sub>0,8,1</sub>	-5.4014	23	0.112	$8.0 \times 10^{-4}$
CH <sub>3</sub> CONH <sub>2</sub>	97.94387	9 <sub>0,9,0,2</sub> → 8 <sub>1,8,0,2</sub>	-4.6386	24	0.050	$4.3 \times 10^{-4}$
CH <sub>3</sub> CONH <sub>2</sub>	97.94387	9 <sub>1,9,0,2</sub> → 8 <sub>1,8,0,2</sub>	-5.8455	24	$3.1 \times 10^{-3}$	$2.7 \times 10^{-5}$
CH <sub>3</sub> CONH <sub>2</sub>	97.94388	9 <sub>0,9,0,2</sub> → 8 <sub>0,8,0,2</sub>	-5.8455	24	$3.1 \times 10^{-3}$	$2.7 \times 10^{-5}$
CH <sub>3</sub> CONH <sub>2</sub>	97.94388	9 <sub>1,9,0,2</sub> → 8 <sub>0,8,0,2</sub>	-4.6386	24	0.050	$4.3 \times 10^{-4}$
N-CH <sub>3</sub> NHCHO	93.40638	9 <sub>0,9,0,0</sub> → 8 <sub>0,8,0,0</sub>	-4.8163	23	0.52	$4.5 \times 10^{-3}$
HCOCH <sub>2</sub> OH	95.07007	9 <sub>1,9,0</sub> → 8 <sub>0,8,0</sub>	-4.4839	23	0.29	$2.5 \times 10^{-3}$
CH <sub>3</sub> COOH	90.24624	8 <sub>0,8,0,1</sub> → 7 <sub>1,7,0,2</sub>	-5.4378	20	0.052	$4.4 \times 10^{-4}$
CH <sub>3</sub> COOH	90.24624	8 <sub>1,8,0,1</sub> → 7 <sub>1,7,0,2</sub>	-5.9027	20	0.0177	$1.52 \times 10^{-4}$
CH <sub>3</sub> COOH	90.24627	8 <sub>0,8,0,1</sub> → 7 <sub>0,7,0,2</sub>	-5.9027	20	0.0177	$1.52 \times 10^{-4}$
CH <sub>3</sub> COOH	90.24627	8 <sub>1,8,0,1</sub> → 7 <sub>0,7,0,2</sub>	-5.4378	20	0.052	$4.4 \times 10^{-4}$
NH <sub>2</sub> CH <sub>2</sub> CH <sub>2</sub> OH	101.86399	10 <sub>1,9,0</sub> → 9 <sub>1,8,0</sub>	-4.5142	28	0.41	$3.6 \times 10^{-3}$
aGg <sup>+</sup> -((CH <sub>2</sub> OH) <sub>2</sub> )	92.97589	9 <sub>1,9,1</sub> → 8 <sub>1,8,0</sub>	-4.6002	22	0.39	$3.4 \times 10^{-3}$
gGg <sup>+</sup> -((CH <sub>2</sub> OH) <sub>2</sub> )	96.68331	10 <sub>0,10,1</sub> → 9 <sub>0,9,0</sub>	-4.7461	26	0.31	$2.7 \times 10^{-3}$
CH <sub>3</sub> OCH <sub>2</sub> OH	90.14764	9 <sub>0,9,1</sub> → 8 <sub>0,8,1</sub>	-6.5734	22	0.073	$6.3 \times 10^{-4}$
CH <sub>3</sub> OCH <sub>2</sub> OH	90.14817	9 <sub>0,9,0</sub> → 8 <sub>0,8,0</sub>	-6.5734	22	0.073	$6.3 \times 10^{-4}$
HOCH <sub>2</sub> C(O)NH <sub>2</sub>	97.61060	5 <sub>5,1</sub> → 4 <sub>4,0</sub>	-4.4215	13.4	0.146	$1.26 \times 10^{-3}$
HOCH <sub>2</sub> C(O)NH <sub>2</sub>	97.61116	5 <sub>5,0</sub> → 4 <sub>4,1</sub>	-4.4215	13.4	0.146	$1.26 \times 10^{-3}$

**Notes.** Frequency is the rest frequency of the transitions in GHz; Transition indicates the quantum numbers;  $\log I$  is the logarithm of the line intensity in nm<sup>2</sup> MHz;  $E_{\text{up}}$  is the energy of the state of higher energy in K; Area is the integrated intensity of the line in K km s<sup>-1</sup> and  $\tau$  is the optical depth of the transition. In case of upper limits, the transitions listed are only those used to retrieve the upper limit (see Fig. S 28).

Table S 2: List of the transitions of the molecules analyzed in this work in G31.41 core that were used to perform the MADCUBA fits (depicted in Table B.3), ordered by increasing molecular mass.

Molecule	Frequency (GHz)	Transition	$\log I$ (nm <sup>2</sup> MHz)	$E_{\text{up}}$ (K)	Area (K km s <sup>-1</sup> )	$\tau$
Detected molecules						
NH <sub>2</sub> D	85.92628	1 <sub>1,1,0</sub> → 1 <sub>0,1,1</sub>	-3.4580	21	171 ± 7	0.094 ± 0.016
NH <sub>2</sub> D	96.04864	11 <sub>4,8,1</sub> → 11 <sub>3,8,0</sub>	-4.2871	1160	12 ± 7	0.006 ± 0.012
NH <sub>2</sub> D	99.11882	5 <sub>2,4,1</sub> → 5 <sub>1,4,0</sub>	-3.1998	260	229 ± 7	0.128 ± 0.018
NH <sub>2</sub> D	103.18705	8 <sub>3,6,1</sub> → 8 <sub>2,6,0</sub>	-4.0407	630	26 ± 7	0.014 ± 0.012
NH <sub>2</sub> D	110.15359	1 <sub>1,1,1</sub> → 1 <sub>0,1,0</sub>	-3.7187	21	74 ± 7	0.040 ± 0.013
H <sub>2</sub> CNH	85.21003	16 <sub>2,15</sub> → 15 <sub>3,12</sub>	-4.6384	450	36 ± 7	0.013 ± 0.009
H <sub>2</sub> CNH	85.27204	15 <sub>2,13</sub> → 16 <sub>1,16</sub>	-5.2046	410	10 ± 7	$(4 \pm 9) \cdot 10^{-3}$
H <sub>2</sub> CNH	87.52742	11 <sub>3,8</sub> → 12 <sub>2,11</sub>	-4.4404	270	61 ± 7	0.022 ± 0.010
H <sub>2</sub> CNH	95.30684	7 <sub>2,5</sub> → 8 <sub>1,8</sub>	-4.4258	118	64 ± 7	0.023 ± 0.010
H <sub>2</sub> CNH	95.50844	18 <sub>3,15</sub> → 17 <sub>4,14</sub>	-4.6130	600	31 ± 7	0.011 ± 0.009
H <sub>2</sub> CNH	105.31268	20 <sub>5,15</sub> → 21 <sub>4,18</sub>	-4.8326	840	15 ± 7	$(5 \pm 9) \cdot 10^{-3}$
H <sub>2</sub> CNH	105.79406	4 <sub>0,4</sub> → 3 <sub>1,3</sub>	-3.9162	31	192 ± 7	0.072 ± 0.012
H <sub>2</sub> CNH	109.89239	8 <sub>1,7</sub> → 7 <sub>2,6</sub>	-4.0279	123	136 ± 7	0.051 ± 0.011
H <sub>2</sub> CNH	110.83656	12 <sub>2,10</sub> → 12 <sub>2,11</sub>	-4.7666	280	23 ± 7	$(8 \pm 9) \cdot 10^{-3}$
H <sub>2</sub> CNH	110.89774	6 <sub>1,5</sub> → 6 <sub>1,6</sub>	-4.7382	75	27 ± 7	0.010 ± 0.009
H <sub>2</sub> CNH	114.55019	17 <sub>2,16</sub> → 16 <sub>3,13</sub>	-4.4596	500	39 ± 7	0.014 ± 0.009
H <sub>2</sub> CNH	115.61473	20 <sub>3,18</sub> → 19 <sub>4,15</sub>	-4.5928	720	25 ± 7	$(9 \pm 9) \cdot 10^{-3}$
N <sup>15</sup> NH <sup>+</sup>	91.20426	1 <sub>1</sub> → 0 <sub>1</sub>	-2.8121	4.4	17 ± 4	0.05 ± 0.04
N <sup>15</sup> NH <sup>+</sup>	91.20599	1 <sub>2</sub> → 0 <sub>1</sub>	-2.5903	4.4	28 ± 4	0.08 ± 0.04
N <sup>15</sup> NH <sup>+</sup>	91.20852	1 <sub>0</sub> → 0 <sub>1</sub>	-3.2892	4.4	6 ± 4	0.02 ± 0.04
CH <sub>3</sub> NH <sub>2</sub>	84.21503	4 <sub>0,0</sub> → 3 <sub>-1,1</sub>	-5.4895	21	17 ± 8	0.02 ± 0.02
CH <sub>3</sub> NH <sub>2</sub>	84.30524	1 <sub>1,5</sub> → 1 <sub>0,5</sub>	-5.3560	6.6	24 ± 8	0.02 ± 0.03
CH <sub>3</sub> NH <sub>2</sub>	84.45456	6 <sub>3,5</sub> → 7 <sub>2,5</sub>	-5.4007	80	16 ± 8	0.02 ± 0.02
CH <sub>3</sub> NH <sub>2</sub>	84.59818	2 <sub>1,5</sub> → 2 <sub>0,5</sub>	-5.3242	10.9	25 ± 8	0.03 ± 0.03
CH <sub>3</sub> NH <sub>2</sub>	85.35010	5 <sub>1,6</sub> → 5 <sub>0,7</sub>	-5.7929	37	8 ± 8	0.01 ± 0.02
CH <sub>3</sub> NH <sub>2</sub>	85.42507	3 <sub>1,5</sub> → 3 <sub>0,5</sub>	-5.4629	17.3	18 ± 8	0.02 ± 0.02
CH <sub>3</sub> NH <sub>2</sub>	86.07473	4 <sub>-1,1</sub> → 4 <sub>0,0</sub>	-4.9718	25	52 ± 8	0.05 ± 0.03
CH <sub>3</sub> NH <sub>2</sub>	86.89871	4 <sub>1,5</sub> → 4 <sub>0,5</sub>	-5.6672	26	11 ± 8	0.01 ± 0.02

Table S 2: Continued.

Molecule	Frequency (GHz)	Transition	$\log I$ (nm <sup>2</sup> MHz)	$E_{\text{up}}$ (K)	Area (K km s <sup>-1</sup> )	$\tau$
CH <sub>3</sub> NH <sub>2</sub>	87.04905	11 <sub>-2,3</sub> → 10 <sub>3,2</sub>	-5.1200	157	22 ± 8	0.02 ± 0.03
CH <sub>3</sub> NH <sub>2</sub>	87.09814	8 <sub>-1,3</sub> → 7 <sub>2,2</sub>	-5.1407	80	28 ± 8	0.03 ± 0.03
CH <sub>3</sub> NH <sub>2</sub>	87.50725	10 <sub>4,5</sub> → 11 <sub>3,5</sub>	-5.2618	180	14 ± 8	0.01 ± 0.02
CH <sub>3</sub> NH <sub>2</sub>	87.78249	3 <sub>1,0</sub> → 3 <sub>0,1</sub>	-5.0561	17.0	44 ± 8	0.04 ± 0.03
CH <sub>3</sub> NH <sub>2</sub>	88.15999	7 <sub>1,5</sub> → 6 <sub>2,4</sub>	-5.5473	65	12 ± 8	0.01 ± 0.02
CH <sub>3</sub> NH <sub>2</sub>	88.86723	11 <sub>-2,1</sub> → 10 <sub>3,0</sub>	-5.5780	157	8 ± 8	0.01 ± 0.02
CH <sub>3</sub> NH <sub>2</sub>	89.08146	2 <sub>-1,1</sub> → 2 <sub>0,0</sub>	-5.1836	10.7	33 ± 8	0.03 ± 0.03
CH <sub>3</sub> NH <sub>2</sub>	89.95607	1 <sub>1,0</sub> → 1 <sub>0,1</sub>	-5.3931	6.4	21 ± 8	0.02 ± 0.03
CH <sub>3</sub> NH <sub>2</sub>	90.57210	15 <sub>3,5</sub> → 14 <sub>4,5</sub>	-5.1512	290	12 ± 8	0.01 ± 0.02
CH <sub>3</sub> NH <sub>2</sub>	91.84843	4 <sub>0,5</sub> → 3 <sub>1,5</sub>	-5.0026	22	46 ± 8	0.05 ± 0.03
CH <sub>3</sub> NH <sub>2</sub>	92.98179	8 <sub>-1,1</sub> → 7 <sub>2,0</sub>	-5.5615	80	10 ± 8	0.01 ± 0.02
CH <sub>3</sub> NH <sub>2</sub>	93.17348	6 <sub>3,2</sub> → 7 <sub>-2,3</sub>	-5.3154	80	18 ± 8	0.02 ± 0.02
CH <sub>3</sub> NH <sub>2</sub>	94.05268	6 <sub>-3,3</sub> → 7 <sub>2,2</sub>	-5.3078	80	18 ± 8	0.02 ± 0.02
CH <sub>3</sub> NH <sub>2</sub>	94.42052	11 <sub>2,5</sub> → 10 <sub>3,5</sub>	-5.0802	157	22 ± 8	0.02 ± 0.03
CH <sub>3</sub> NH <sub>2</sub>	94.46620	4 <sub>0,7</sub> → 3 <sub>1,6</sub>	-5.5444	22	13 ± 8	0.01 ± 0.02
CH <sub>3</sub> NH <sub>2</sub>	94.89000	8 <sub>1,4</sub> → 7 <sub>2,5</sub>	-5.5071	80	11 ± 8	0.01 ± 0.02
CH <sub>3</sub> NH <sub>2</sub>	95.14581	4 <sub>0,2</sub> → 3 <sub>-1,3</sub>	-4.9067	22	55 ± 8	0.06 ± 0.03
CH <sub>3</sub> NH <sub>2</sub>	97.48473	15 <sub>3,4</sub> → 14 <sub>4,4</sub>	-5.0893	290	12 ± 8	0.01 ± 0.02
CH <sub>3</sub> NH <sub>2</sub>	99.12725	4 <sub>0,5</sub> → 3 <sub>1,4</sub>	-5.7324	22	8 ± 8	0.01 ± 0.02
CH <sub>3</sub> NH <sub>2</sub>	100.07126	13 <sub>5,4</sub> → 14 <sub>4,4</sub>	-5.2055	290	9 ± 8	0.01 ± 0.02
CH <sub>3</sub> NH <sub>2</sub>	103.66875	8 <sub>1,4</sub> → 7 <sub>2,4</sub>	-5.1845	80	22 ± 8	0.02 ± 0.03
CH <sub>3</sub> NH <sub>2</sub>	104.80014	6 <sub>3,4</sub> → 7 <sub>2,4</sub>	-5.2136	80	20 ± 8	0.02 ± 0.03
CH <sub>3</sub> NH <sub>2</sub>	109.38249	15 <sub>3,2</sub> → 14 <sub>-4,3</sub>	-4.9873	290	14 ± 8	0.01 ± 0.02
CH <sub>3</sub> NH <sub>2</sub>	110.03533	15 <sub>-3,3</sub> → 14 <sub>4,2</sub>	-4.9819	290	14 ± 8	0.01 ± 0.02
CH <sub>3</sub> NH <sub>2</sub>	110.53330	13 <sub>5,5</sub> → 14 <sub>4,5</sub>	-5.1194	290	10 ± 8	0.01 ± 0.02
CH <sub>3</sub> NH <sub>2</sub>	112.27303	13 <sub>-5,3</sub> → 14 <sub>4,2</sub>	-5.1048	290	10 ± 8	0.01 ± 0.02
CH <sub>3</sub> NH <sub>2</sub>	112.28007	13 <sub>5,2</sub> → 14 <sub>-4,3</sub>	-5.1047	290	10 ± 8	0.01 ± 0.02
CH <sub>3</sub> NH <sub>2</sub>	112.59118	9 <sub>-4,3</sub> → 10 <sub>3,2</sub>	-5.0951	158	18 ± 8	0.02 ± 0.02
CH <sub>3</sub> NH <sub>2</sub>	112.65252	9 <sub>4,2</sub> → 10 <sub>-3,3</sub>	-5.0946	158	18 ± 8	0.02 ± 0.02
CH <sub>3</sub> NH <sub>2</sub>	114.12690	25 <sub>2,4</sub> → 25 <sub>1,5</sub>	-4.5982	710	6 ± 8	0.01 ± 0.02
CH <sub>3</sub> NH <sub>2</sub>	114.65860	1 <sub>1,7</sub> → 0 <sub>0,7</sub>	-5.6914	6.1	8 ± 8	0.01 ± 0.02
CH <sub>3</sub> NH <sub>2</sub>	115.83730	2 <sub>2,2</sub> → 3 <sub>-1,3</sub>	-5.6681	23	8 ± 8	0.01 ± 0.02
H <sub>2</sub> CCO	100.09451	5 <sub>1,5</sub> → 4 <sub>1,4</sub>	-3.7629	27	254 ± 5	0.25 ± 0.03
H <sub>2</sub> CCO	100.96735	5 <sub>4,1</sub> → 4 <sub>4,0</sub>	-4.9417	220	8 ± 5	0.007 ± 0.015
H <sub>2</sub> CCO	100.96735	5 <sub>4,2</sub> → 4 <sub>4,1</sub>	-4.9417	220	8 ± 5	0.007 ± 0.015
H <sub>2</sub> CCO	101.00236	5 <sub>3,3</sub> → 4 <sub>3,2</sub>	-4.0824	132	82 ± 5	0.076 ± 0.017
H <sub>2</sub> CCO	101.00236	5 <sub>3,2</sub> → 4 <sub>3,1</sub>	-4.0824	132	82 ± 5	0.076 ± 0.017
H <sub>2</sub> CCO	101.02442	5 <sub>2,4</sub> → 4 <sub>2,3</sub>	-4.3469	67	59 ± 5	0.054 ± 0.016
H <sub>2</sub> CCO	101.03224	5 <sub>2,3</sub> → 4 <sub>2,2</sub>	-4.3468	67	59 ± 5	0.054 ± 0.016
H <sub>2</sub> CCO	101.03663	5 <sub>0,5</sub> → 4 <sub>0,4</sub>	-4.1955	14.5	103 ± 5	0.095 ± 0.018
H <sub>2</sub> CCO	101.98143	5 <sub>1,4</sub> → 4 <sub>1,3</sub>	-3.7471	28	258 ± 5	0.25 ± 0.03
NS	115.15394	3 <sub>1,3,4</sub> → 2 <sub>-1,2,3</sub>	-3.3836	8.8	118 ± 8	0.34 ± 0.09
NS	115.15681	3 <sub>1,3,3</sub> → 2 <sub>-1,2,2</sub>	-3.5843	8.8	77 ± 7	0.21 ± 0.08
NS	115.16298	3 <sub>1,3,2</sub> → 2 <sub>-1,2,1</sub>	-3.8096	8.8	47 ± 7	0.13 ± 0.07
NS	115.18534	3 <sub>1,3,2</sub> → 2 <sub>-1,2,2</sub>	-4.3045	8.8	16 ± 7	0.04 ± 0.07
NS	115.19146	3 <sub>1,3,3</sub> → 2 <sub>-1,2,3</sub>	-4.3045	8.8	16 ± 7	0.04 ± 0.07
NS	115.55625	3 <sub>-1,3,4</sub> → 2 <sub>1,2,3</sub>	-3.3807	8.9	118 ± 8	0.34 ± 0.09
NS	115.57076	3 <sub>-1,3,3</sub> → 2 <sub>1,2,2</sub>	-3.5814	8.9	77 ± 7	0.21 ± 0.08
NS	115.57195	3 <sub>-1,3,2</sub> → 2 <sub>1,2,1</sub>	-3.8067	8.9	47 ± 7	0.13 ± 0.07
Non detected molecules						
HC <sup>17</sup> O <sup>+</sup>	87.05753	1 → 0	-2.2763	4.2	6.4	0.0120
c-C <sub>3</sub> H <sub>2</sub>	102.50596	9 <sub>6,3</sub> → 9 <sub>5,4</sub>	-3.2251	137	58	0.054
HCS <sup>+</sup>	85.34789	2 → 1	-2.9031	6.1	36	0.106
HC <sub>5</sub> N	114.48503	43 → 42	-1.99550	121	26	0.024

**Notes.** Frequency is the rest frequency of the transitions in GHz; Transition indicates the quantum numbers;  $\log I$  is the logarithm of the line intensity in nm<sup>2</sup> MHz;  $E_{\text{up}}$  is the energy of the state of higher energy in K; Area is the integrated intensity of the line in K km s<sup>-1</sup> and  $\tau$  is the optical depth of the transition. In case of upper limits, the transitions listed are only those used to retrieve the upper limit (see Fig. S 35).

### S 3. Spectra of detected molecules toward the G31.41 shock

We show here the spectra of the detected molecules toward G31.41 shock. The results of the parameters obtained from the fits are summarized in Table B.1 and Table B.2, and the information about the transitions used is listed in Table S 1.

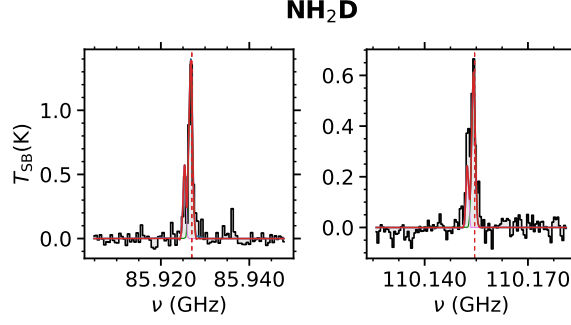


Fig. S 1: Transitions of NH<sub>2</sub>D detected toward the G31.41 shock position. The black histogram and its gray shadow are the observed spectrum. There are two components fitted (the pink and green curves) which are the best LTE fit of the individual species, the red curve is the sum of the two components, and the blue curve is the cumulative fit considering all detected species. The red dashed lines indicate the frequency of the transitions that we are fitting. The plots are sorted by decreasing line intensity of the transitions.

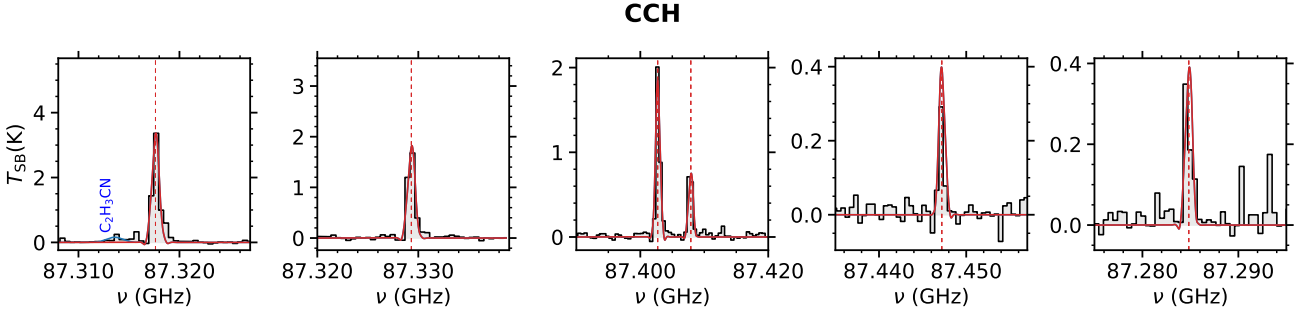


Fig. S 2: Transitions of CCH detected toward the G31.41 shock position. The black histogram and its gray shadow are the observed spectrum. The red curve is the best LTE fit of the individual species and the blue curve is the cumulative fit considering all detected species. The red dashed lines indicate the frequency of the transitions that we are fitting. The plots are sorted by decreasing line intensity of the transitions.

### S 4. Spectra of molecules not detected toward G31.41 shock

The spectra of the transitions used to obtain the column density upper limits toward G31.41 shock, presented in Table B.1, are shown in Fig. S 28, and the information about the transitions used is included in Table S 1. The upper limits are calculated by using the upper limit tool of MADCUBA (explained in more detail in Sect. 3.2.1).

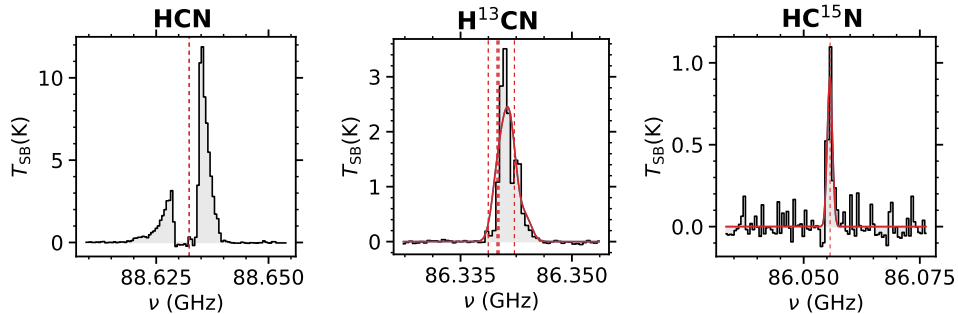


Fig. S 3: Transitions of HCN isotopologs detected toward the G31.41 shock position. The black histogram and its gray shadow are the observed spectrum. The red curve is the best LTE fit of the individual species and the blue curve is the cumulative fit considering all detected species. The red dashed lines indicate the frequency of the transitions that we are fitting. The plots are sorted by decreasing line intensity of the transitions.

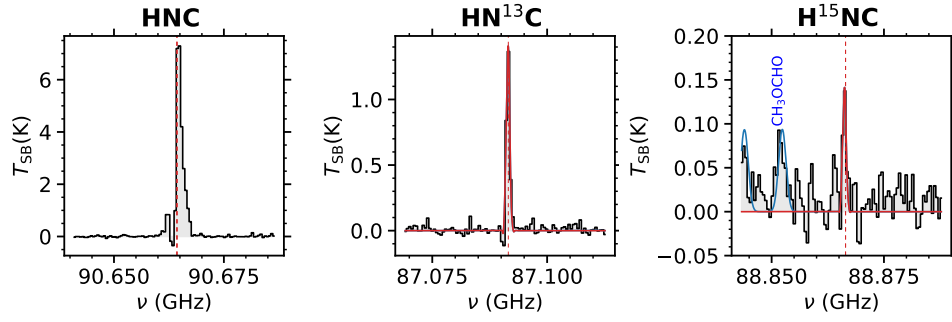


Fig. S 4: Transitions of HNC isotopologs detected toward the G31.41 shock position. The black histogram and its gray shadow are the observed spectrum. The red curve is the best LTE fit of the individual species and the blue curve is the cumulative fit considering all detected species. The red dashed lines indicate the frequency of the transitions that we are fitting. The plots are sorted by decreasing line intensity of the transitions.

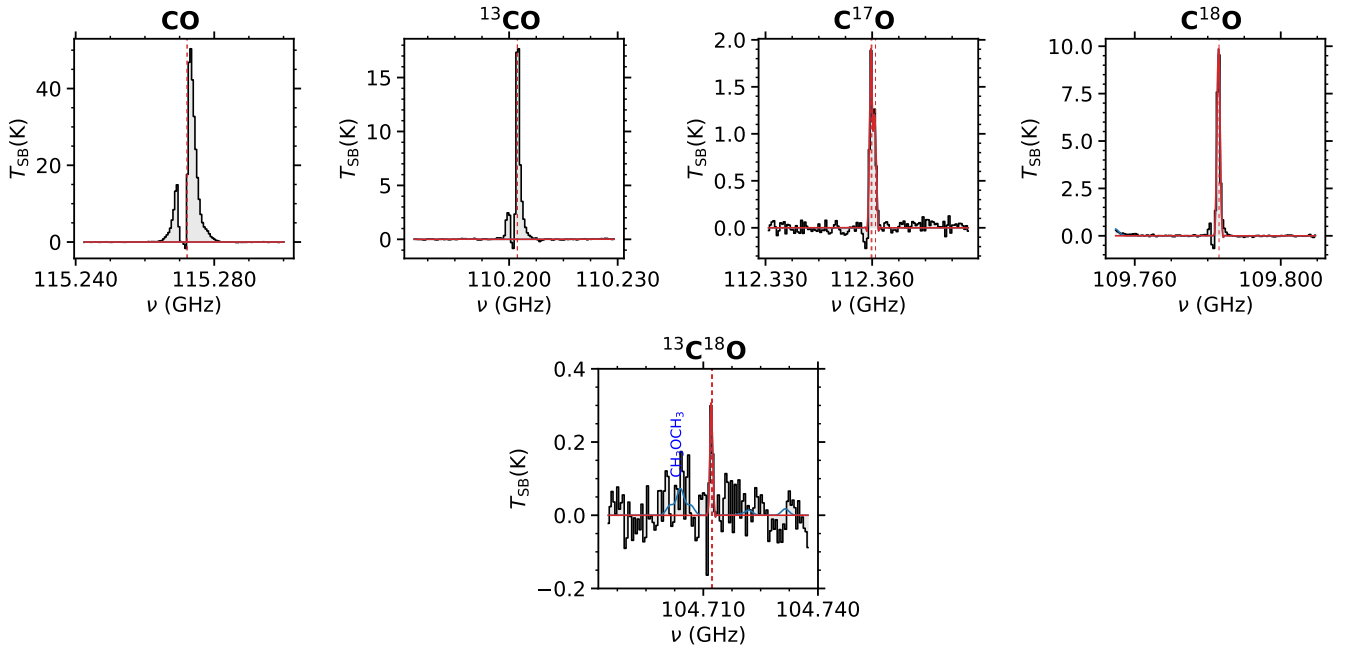


Fig. S 5: Transitions of CO isotopologs detected toward the G31.41 shock position. The black histogram and its gray shadow are the observed spectrum. The red curve is the best LTE fit of the individual species and the blue curve is the cumulative fit considering all detected species. The red dashed lines indicate the frequency of the transitions that we are fitting. The plots are sorted by decreasing line intensity of the transitions.

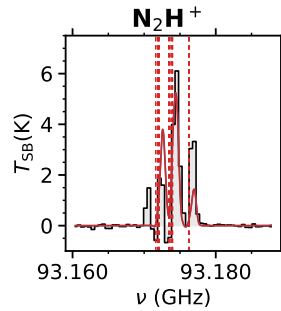


Fig. S 6: Transitions of  $\text{N}_2\text{H}^+$  detected toward the G31.41 shock position. The black histogram and its gray shadow are the observed spectrum. The red curve is the best LTE fit of the individual species and the blue curve is the cumulative fit considering all detected species. The red dashed lines indicate the frequency of the transitions that we are fitting. The plots are sorted by decreasing line intensity of the transitions.

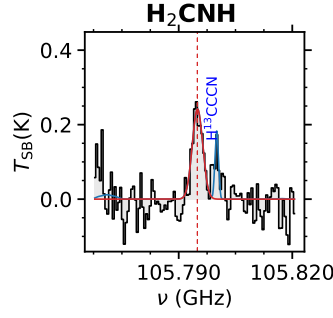


Fig. S 7: Transition of  $\text{H}_2\text{CNH}$  detected toward the G31.41 shock position. The black histogram and its gray shadow are the observed spectrum. The red curve is the best LTE fit of the individual species and the blue curve is the cumulative fit considering all detected species. The red dashed lines indicate the frequency of the transitions that we are fitting. The plots are sorted by decreasing line intensity of the transitions.

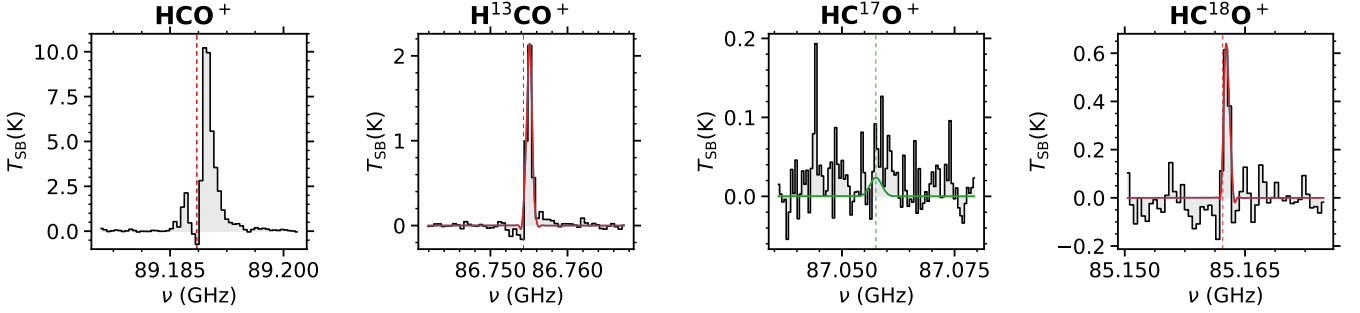


Fig. S 8: Transitions of  $\text{HCO}^+$  isotopologs detected toward the G31.41 shock position. The black histogram and its gray shadow are the observed spectrum. The red curve is the best LTE fit of the individual species and the blue curve is the cumulative fit considering all detected species. The LTE synthetic spectra using the derived upper limits of  $N$  are indicated with green curves. The red/green dashed lines indicate the frequency of the transitions that we are fitting. The plots are sorted by decreasing line intensity of the transitions.

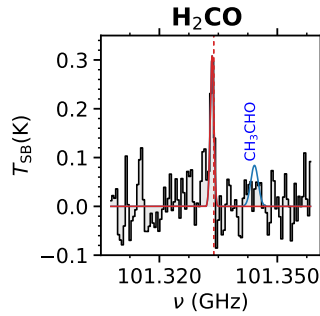


Fig. S 9: Transitions of  $\text{H}_2\text{CO}$  detected toward the G31.41 shock position. The black histogram and its gray shadow are the observed spectrum. The red curve is the best LTE fit of the individual species and the blue curve is the cumulative fit considering all detected species. The red dashed lines indicate the frequency of the transitions that we are fitting. The plots are sorted by decreasing line intensity of the transitions.

## S 5. Spectroscopic catalog entries

Table S 3 lists the spectroscopic catalog entries of all the molecules analyzed in this work toward the G31.41 shock. The species are ordered by increasing molecular mass.

Table S 3: Spectroscopic entries used to perform the analysis, including the molecular catalog, tag of the species, version number, and date of the version.

Formula	Name	Mol. mass	Catalogue	Tag	Version	Date version
Detected molecules						
$\text{NH}_2\text{D}$	Deuterated Ammonia	18	CDMS	18501	1	May 2004

Table S 3: Continued.

Formula	Name	Mol. mass	Catalog	TAG	Version	Date version
CCH	Ethynyl	25	CDMS	25501	3	July 2010
HCN	Hydrogen cyanide	27	CDMS	27501	4	May 2007
H <sup>13</sup> CN			CDMS	28501	3	Nov. 2014
HC <sup>15</sup> N			CDMS	28506	2	Dec. 2017
HNC			CDMS	27502	2	Feb. 2005
HN <sup>13</sup> C	Hydrogen isocyanide	27	CDMS	28515	1	Sep. 2009
H <sup>15</sup> NC			JPL	28006	1	Dec. 1979
C <sup>17</sup> O			CDMS	29503	1	Jan 2003
C <sup>18</sup> O	Carbon monoxide	28	CDMS	30502	1	June 2001
<sup>13</sup> C <sup>18</sup> O			CDMS	31502	1	July 2000
H <sub>2</sub> CNH	Methanimine	29	CDMS	29518	2	May 2014
N <sub>2</sub> H <sup>+</sup>	Diazenylium	29	CDMS	29506	4	Apr. 2014
HCO <sup>+</sup>	Oxomethylum	29	CDMS	29507	2	Oct. 2007
HC <sup>18</sup> O <sup>+</sup>			CDMS	31506	1	Dec. 2004
H <sup>13</sup> CO <sup>+</sup>			CDMS	30504	2	Oct. 2007
H <sub>2</sub> CO	Formaldehyde	30	CDMS	30501	3	Feb. 2017
CH <sub>3</sub> OH	Methanol	32	CDMS	32504	3	May 2016
c-C <sub>3</sub> H <sub>2</sub>	Cyclopropenylidene	38	JPL	38002	2	Jan. 1996
CH <sub>3</sub> CCH	Propyne	40	CDMS	40502	3	Aug. 2008
CH <sub>3</sub> CN	Methyl isocyanide	41	CDMS	41505	1	Aug. 2018
NH <sub>2</sub> CN	Cyanamide	42	JPL	42003	1	Jan. 1991
H <sub>2</sub> CCO	Ketene	42	CDMS	42501	2	Nov. 2003
HNCO	Isocyanic acid	43	JPL	43002	1	July 1987
CH <sub>3</sub> CHO	Acetaldehyde	43	JPL	44003	3	Jan. 2012
<sup>13</sup> CS	Carbon monosulfide	44	CDMS	45501	2	Jan. 2004
<sup>13</sup> C <sup>34</sup> S			CDMS	47501	2	Jan. 2004
C <sup>34</sup> S			CDMS	46501	2	Jan. 2004
C <sup>33</sup> S			CDMS	45502	2	Jan. 2004
C <sup>36</sup> S			CDMS	48503	2	Jan. 2004
NH <sub>2</sub> CHO	Formamide	45	JPL	45003	2	Jan. 1981
HCS <sup>+</sup>	Thiomethylum/thioformyl cation	45	CDMS	45506	1	June 2003
H <sub>2</sub> CS	Thioformaldehyde	46	CDMS	42517	1	Sep. 2017
H <sub>2</sub> <sup>13</sup> CS			CDMS	47505	2	Jan. 2019
H <sub>2</sub> C <sup>33</sup> S			CDMS	47506	2	Jan. 2019
H <sub>2</sub> C <sup>34</sup> S			CDMS	48508	2	Jan. 2019
C <sub>2</sub> H <sub>5</sub> OH	Ethanol	46	CDMS	46524	1	Nov. 2016
CH <sub>3</sub> OCH <sub>3</sub>	Dimethyl ether	46	CDMS	43510	1	May. 2009
NS	Nitrogen Sulfide	46	CDMS	46515	1	Aug 2011
CH <sub>3</sub> SH	Methyl mercaptan	48	CDMS	48510	2	May 2020
HC <sub>3</sub> N	Cyanoacetylene	51	CDMS	51501	1	Oct. 2000
H <sup>13</sup> CCCN			CDMS	52509	1	Dec. 2004
HC <sup>13</sup> CCN			CDMS	52510	1	Dec. 2004
HCC <sup>13</sup> CN			CDMS	52511	1	Dec. 2004
C <sub>2</sub> H <sub>3</sub> CN	Vinyl cyanide	53	CDMS	53515	1	May 2008
OCS	Carbonyl sulfide	60	CDMS	60503	2	Nov. 2005
CH <sub>3</sub> OCHO	Methyl formate	60	JPL	60003	1	Apr. 2009
HC <sub>5</sub> N	Cyanodiacetylene	75	CDMS	75503	2	Aug. 2020
Non detected molecules (upper limits)						
HC <sup>17</sup> O <sup>+</sup>	Formaldehyde	30	CDMS	30505	1	Feb. 2004
CH <sub>3</sub> NH <sub>2</sub>	Methylamine	31	LSD	31801	1	Aug. 2021
CH <sub>3</sub> NC	Methyl isocyanide	41	CDMS	41514	1	Aug. 2018
HOCN	Cyanic acid	43	CDMS	43510	1	May. 2009
c-C <sub>2</sub> H <sub>4</sub> O	Ethylene oxide	44	CDMS	44504	3	Mar. 2022
t-HCOOH	Formic acid	46	CDMS	46506	1	July 2003
trans-HONO	Nitrous acid	47	JPL	47007	1	Jan. 2006
Z-HNCHCN	Cyanometanimine	54	CDMS	54513	2	Nov. 2018
C <sub>2</sub> H <sub>5</sub> CHO	Propanal	55	CDMS	55502	2	Aug. 2009
CH <sub>3</sub> NCO	Methyl Isocyanate	57	CDMS	57505	1	Mar. 2016

Table S 3: Continued.

Formula	Name	Mol. mass	Catalog	TAG	Version	Date version
C <sub>2</sub> H <sub>5</sub> CHO	Propanal	58	CDMS	58505	2	Jan. 2018
CH <sub>3</sub> COCH <sub>3</sub>	Acetone	58	JPL	58003	1	Mar. 2008
CH <sub>3</sub> CONH <sub>2</sub>	Acetamide	59	USER			
N-CH <sub>3</sub> NHCHO	N-Methylformamide	59	USER			
HCOCH <sub>2</sub> OH	Glycolaldehyde	60	JPL	60006	2	June 2012
CH <sub>3</sub> COOH	Acetic acid	60	CDMS	60523	1	May 2019
NH <sub>2</sub> CH <sub>2</sub> CH <sub>2</sub> OH	Ethanolamine	61	JPL	61004	3	Sep. 2003
aGg'-(CH <sub>2</sub> OH) <sub>2</sub>	aGg'- Ethylene glycol	62	CDMS	62503	1	Sep. 2003
gGg'-(CH <sub>2</sub> OH) <sub>2</sub>	gGg'- Ethylene glycol	62	CDMS	62504	1	May 2004
CH <sub>3</sub> OCH <sub>2</sub> OH	Methoxymethanol	62	CDMS	62527	1	Aug. 2020
HOCH <sub>2</sub> C(O)NH <sub>2</sub>	Glycolamide	75	CDMS	75517	1	Dec. 2020

## S 6. LTE fits of additional molecules detected in the G31.41 core

In the following subsections, we describe the LTE fit of all the additional detected molecules in the G31.41 core of this work, whose results are summarized in Table B.3. The transitions used for each detected molecule are depicted in Table S 1 and they are plotted in Appendix S 7.

### S 6.1. Deuterated Ammonia (NH<sub>2</sub>D)

The transitions  $5_{2,4,1} \rightarrow 5_{1,4,0}$  and  $8_{3,6,1} \rightarrow 8_{2,6,0}$  of NH<sub>2</sub>D are completely unblended (see Fig. S 29). Transitions  $1_{1,1,0} \rightarrow 1_{0,1,1}$ ,  $11_{4,8,1} \rightarrow 11_{3,8,0}$  and  $1_{1,1,1} \rightarrow 1_{0,1,0}$  are blended with CH<sub>3</sub>OCHO but the transitions help to reproduce the observed spectrum. By fixing the FWHM to 7 km s<sup>-1</sup> (see Table B.3), the transitions of the obtained fit are optically thin ( $\tau < 0.13$ , see Table S 1) and the resultant column density is  $3.8 \times 10^{16}$  cm<sup>-2</sup> for NH<sub>2</sub>D.

### S 6.2. Methanimine (H<sub>2</sub>CNH)

The 5 brightest transitions of H<sub>2</sub>CNH are completely unblended strengthening the detection (see Fig. S 30). The transitions  $20_{3,18} \rightarrow 19_{4,15}$  and  $12_{2,10} \rightarrow 12_{2,11}$  are contaminated with n-C<sub>3</sub>H<sub>7</sub>CN and C<sub>2</sub>H<sub>3</sub>CN respectively, but they help to reproduce the observed spectrum. The transitions from the fit are optically thin ( $\tau < 0.072$ , see Table S 1) and the temperature converged to  $254 \pm 20$  K. We obtain a column density value of  $1.5 \times 10^{17}$  cm<sup>-2</sup> for H<sub>2</sub>CNH. This value is almost an order of magnitude higher in terms of column density than the one observed by Suzuki et al. (2023) at higher frequency with ALMA bands 5 and 6 which is  $(3.5 \pm 0.2) \times 10^{16}$  cm<sup>-2</sup>.

### S 6.3. Diazenylium (N<sub>2</sub>H<sup>+</sup>)

The transitions of N<sub>2</sub>H<sup>+</sup> are in absorption, thus to obtain the column density of the main isotopolog, we use the available isotopologs: <sup>15</sup>NNH<sup>+</sup> and N<sup>15</sup>NH<sup>+</sup>, which are contaminated with <sup>13</sup>CH<sub>3</sub>OH and HC<sub>3</sub>N, respectively (see Fig. S 31). We choose N<sup>15</sup>NH<sup>+</sup> because is less contaminated and the fit is optically thin ( $\tau < 0.082$ , see Table S 1). The fit of N<sup>15</sup>NH<sup>+</sup> converged by fixing the temperature to 50 K and the FWHM to 7 km s<sup>-1</sup>. Using the <sup>14</sup>N/<sup>15</sup>N isotopic ratio explained in Sect. 3.2.2, we derive a column density of  $7 \times 10^{16}$  cm<sup>-2</sup> for N<sub>2</sub>H<sup>+</sup>.

### S 6.4. Methyl Amine (CH<sub>3</sub>NH<sub>2</sub>)

The 4 most intense transitions of CH<sub>3</sub>NH<sub>2</sub> are unblended (see Fig. S 32). The rest of the transitions are blended but they are necessary to mimic the observed spectrum. Due to the high amount of transitions used for this fit, the detection is strong. By letting fixed the FWHM to 7 km s<sup>-1</sup> (see Table B.3), the fit shows that the transitions are optically thin ( $\tau < 0.05$ , see Table S 1). We obtain a column density of  $1.8 \times 10^{17}$  cm<sup>-2</sup>. This value is identical with the one obtained by Suzuki et al. (2023), which is  $(1.8 \pm 0.1) \times 10^{17}$  cm<sup>-2</sup> with bands 5 and 6 of ALMA.

### S 6.5. Ketene (H<sub>2</sub>CCO)

The  $5_{1,5} \rightarrow 4_{1,4}$  and  $5_{1,4} \rightarrow 4_{1,4}$  transitions of H<sub>2</sub>CCO are unblended (see Fig. S 33). The other transitions are blended but they help to reproduce the observed spectrum. The LTE fit converged by letting free all the parameters, strengthening the detection. The resultant transitions are almost optically thin ( $\tau < 0.25$ , see Table S 1). The column density obtained is  $6 \times 10^{16}$  cm<sup>-2</sup>.



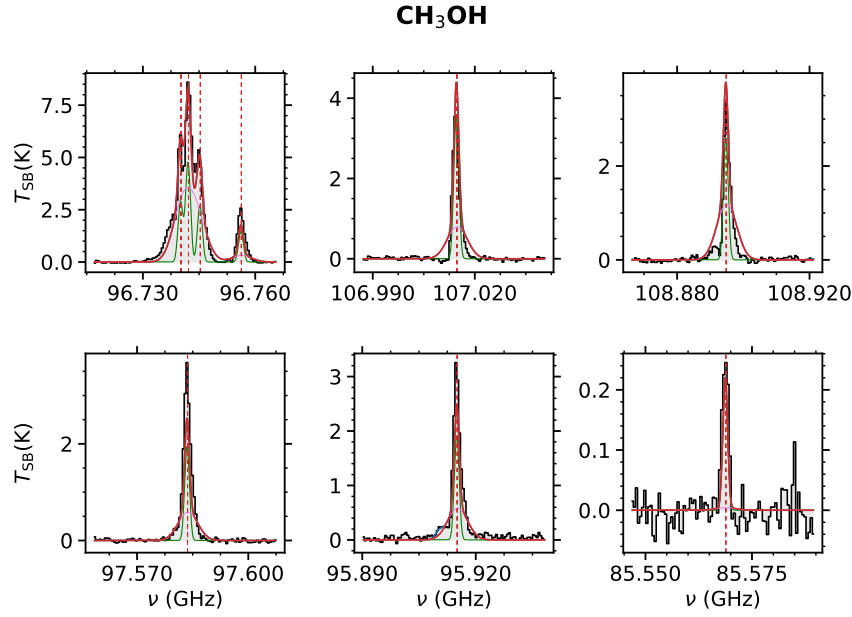


Fig. S 10: Transitions of CH<sub>3</sub>OH detected toward the G31.41 shock position. The black histogram and its gray shadow are the observed spectrum. There are two components fitted (the pink and green curves) which are the best LTE fit of the individual species, the red curve is the sum of the two components, and the blue curve is the cumulative fit considering all detected species. The red dashed lines indicate the frequency of the transitions that we are fitting. The plots are sorted by decreasing line intensity of the transitions.

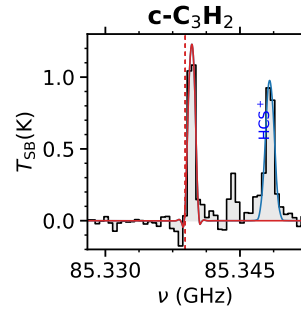


Fig. S 11: Transitions of c-C<sub>3</sub>H<sub>2</sub> detected toward the G31.41 shock position. The black histogram and its gray shadow are the observed spectrum. The red curve is the best LTE fit of the individual species and the blue curve is the cumulative fit considering all detected species. The red dashed lines indicate the frequency of the transitions that we are fitting. The plots are sorted by decreasing line intensity of the transitions.

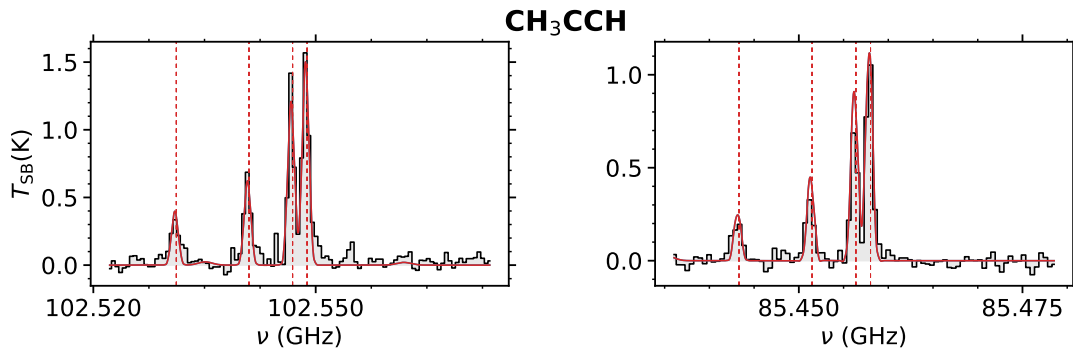


Fig. S 12: Transitions of CH<sub>3</sub>CCH detected toward the G31.41 shock position. The black histogram and its gray shadow are the observed spectrum. The red curve is the best LTE fit of the individual species and the blue curve is the cumulative fit considering all detected species. The red dashed lines indicate the frequency of the transitions that we are fitting. The plots are sorted by decreasing line intensity of the transitions.

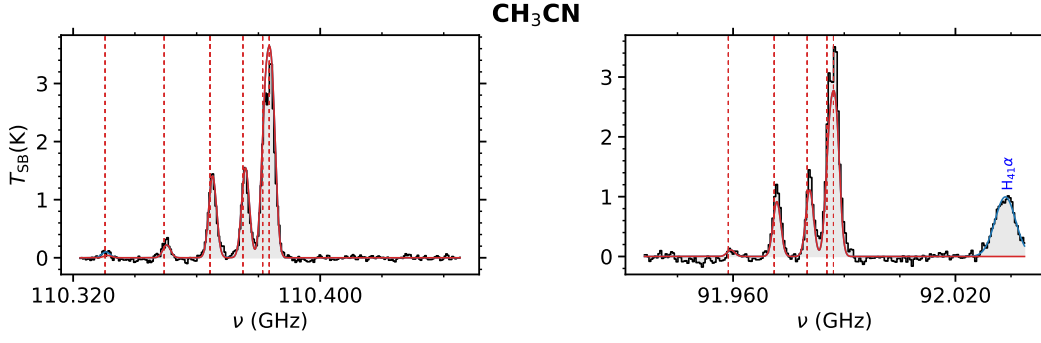


Fig. S 13: Transitions of  $\text{CH}_3\text{CN}$  detected toward the G31.41 shock position. The black histogram and its gray shadow are the observed spectrum. The red curve is the best LTE fit of the individual species and the blue curve is the cumulative fit considering all detected species. The red dashed lines indicate the frequency of the transitions that we are fitting. The plots are sorted by decreasing line intensity of the transitions.

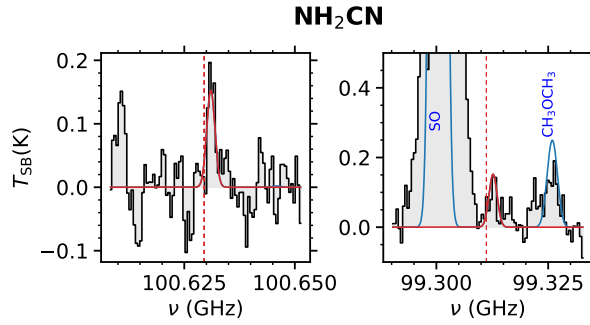


Fig. S 14: Transitions of  $\text{NH}_2\text{CN}$  detected toward the G31.41 shock position. The black histogram and its gray shadow are the observed spectrum. The red curve is the best LTE fit of the individual species and the blue curve is the cumulative fit considering all detected species. The red dashed lines indicate the frequency of the transitions that we are fitting. The plots are sorted by decreasing line intensity of the transitions.

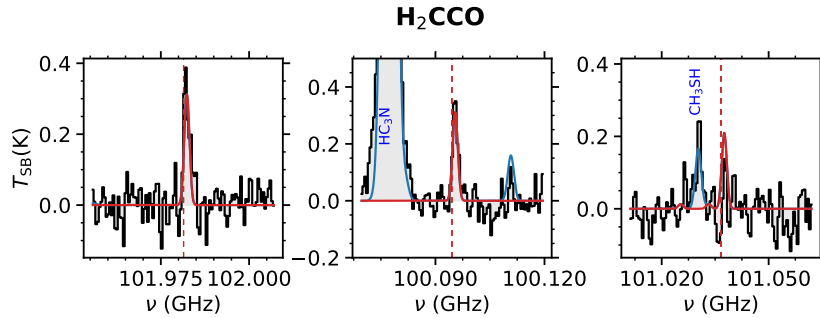


Fig. S 15: Transitions of  $\text{H}_2\text{CCO}$  detected toward the G31.41 shock position. The black histogram and its gray shadow are the observed spectrum. The red curve is the best LTE fit of the individual species and the blue curve is the cumulative fit considering all detected species. The red dashed lines indicate the frequency of the transitions that we are fitting. The plots are sorted by decreasing line intensity of the transitions.

### S 6.6. Nitrogen Sulfide (NS)

The  $3_{-1,3,3} \rightarrow 2_{1,2,2}$  and  $3_{-1,3,2} \rightarrow 2_{1,2,1}$  transitions of NS are unblended (see Fig. S 34). The  $3_{-1,3,4} \rightarrow 2_{1,2,3}$ ,  $3_{1,3,4} \rightarrow 2_{-1,2,3}$  and  $3_{1,3,3} \rightarrow 2_{-1,2,2}$  transitions are blended with  $\text{CH}_3\text{OCHO}$  but they help to reproduce the observed spectrum. The NS fit converged by fixing the temperature to 50 K and the velocity to 96.5 km s<sup>-1</sup> (see Table B.3). The transitions are slightly optically thick ( $\tau < 0.34$ , see Table S 1). The NS column density obtained is  $6.1 \times 10^{15}$  cm<sup>-2</sup>. We checked the  $\text{N}^{33}\text{S}$  and  $\text{N}^{34}\text{S}$  isotopologues but they are too faint to be detected.

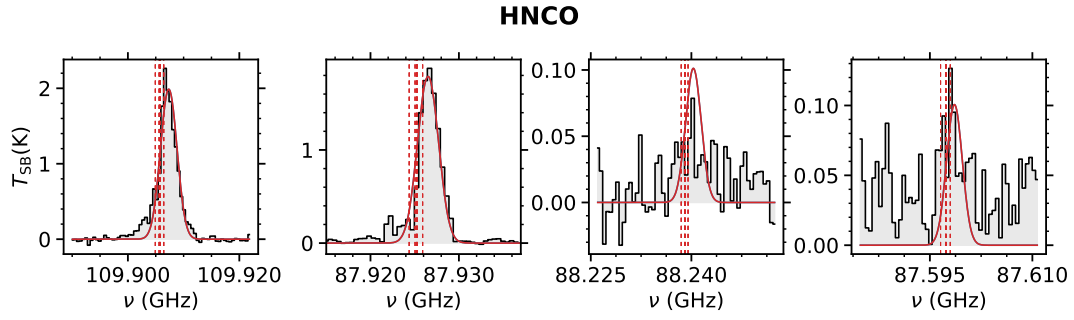


Fig. S 16: Transitions of HNCO detected toward the G31.41 shock position. The black histogram and its gray shadow are the observed spectrum. The red curve is the best LTE fit of the individual species and the blue curve is the cumulative fit considering all detected species. The red dashed lines indicate the frequency of the transitions that we are fitting. The plots are sorted by decreasing line intensity of the transitions.

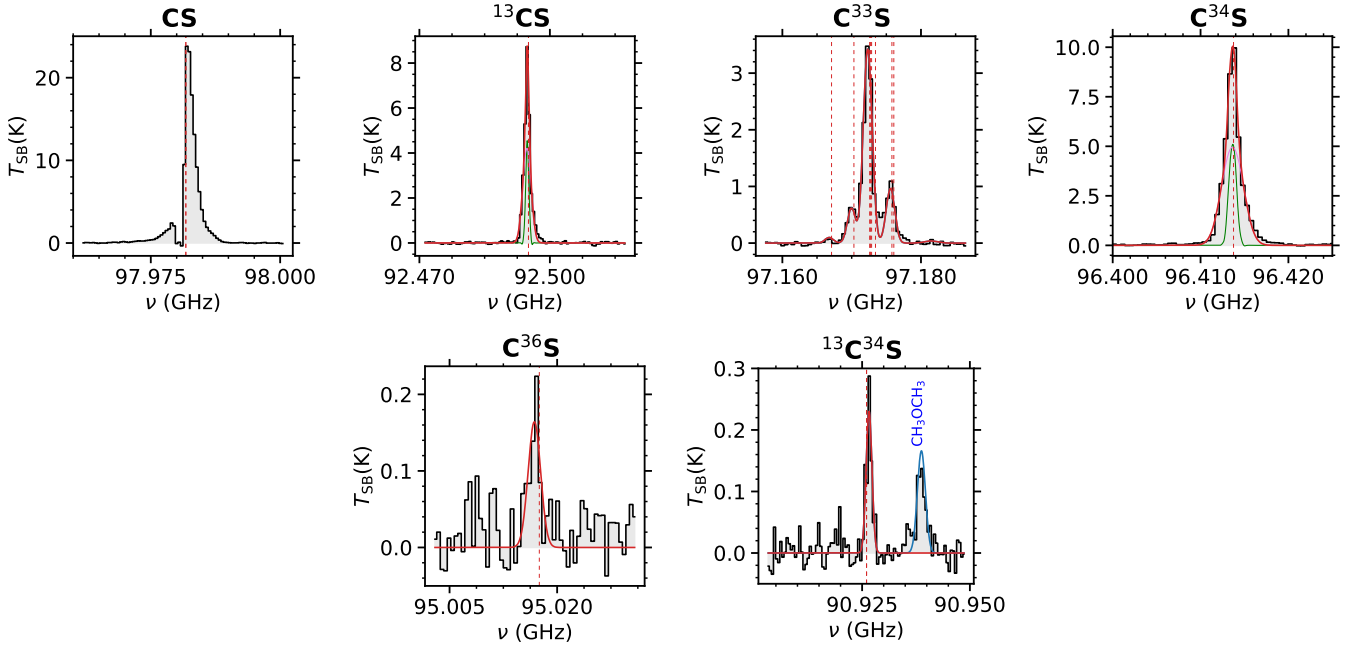


Fig. S 17: Transitions of CS isotopologs detected toward the G31.41 shock position. The black histogram and its gray shadow are the observed spectrum. The red curve is the best LTE fit of the individual species and the blue curve is the cumulative fit considering all detected species. The red dashed lines indicate the frequency of the transitions that we are fitting. The plots are sorted by decreasing line intensity of the transitions. For  $^{13}\text{CS}$  and  $\text{C}^{34}\text{S}$ , we used two components to fit, plotted in pink and green. In these cases, the red curve is the sum of both components.

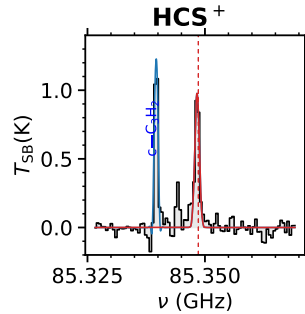


Fig. S 18: Transitions of  $\text{HCS}^+$  detected toward the G31.41 shock position. The black histogram and its gray shadow are the observed spectrum. The red curve is the best LTE fit of the individual species and the blue curve is the cumulative fit considering all detected species. The red dashed lines indicate the frequency of the transitions that we are fitting. The plots are sorted by decreasing line intensity of the transitions.

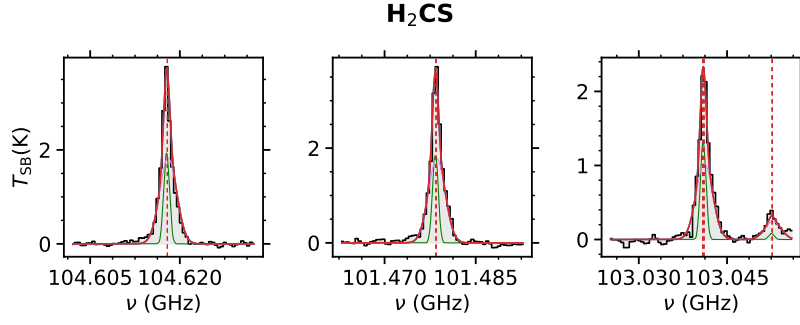


Fig. S 19: Transitions of H<sub>2</sub>CS detected toward the G31.41 shock position. The black histogram and its gray shadow are the observed spectrum. There are two components fitted (the pink and green curves) which are the best LTE fit of the individual species, the red curve is the sum of the two components and the blue curve is the cumulative fit considering all detected species. The red dashed lines indicate the frequency of the transitions that we are fitting. The plots are sorted by decreasing line intensity of the transitions.

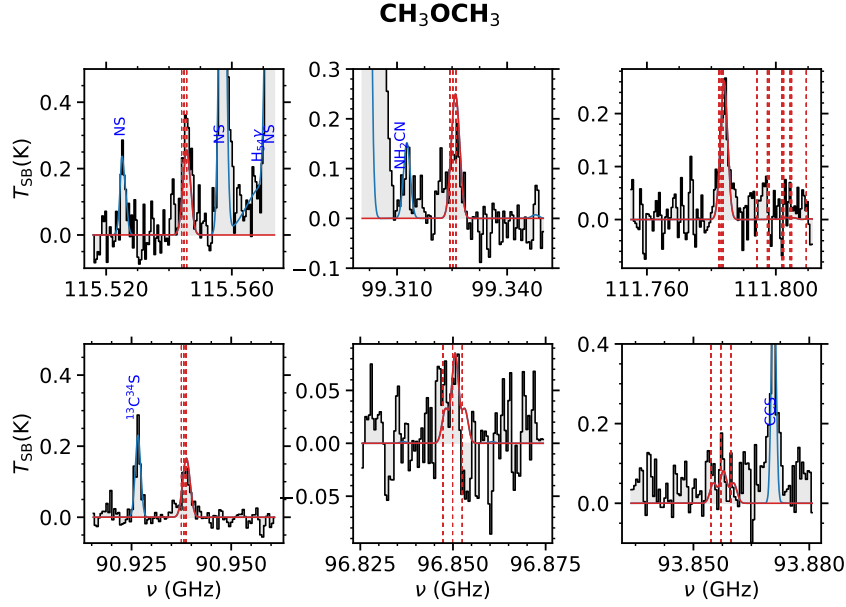


Fig. S 20: Transitions of CH<sub>3</sub>OCH<sub>3</sub> detected toward the G31.41 shock position. The black histogram and its gray shadow are the observed spectrum. The red curve is the best LTE fit of the individual species and the blue curve is the cumulative fit considering all detected species. The red dashed lines indicate the frequency of the transitions that we are fitting. The plots are sorted by decreasing line intensity of the transitions.

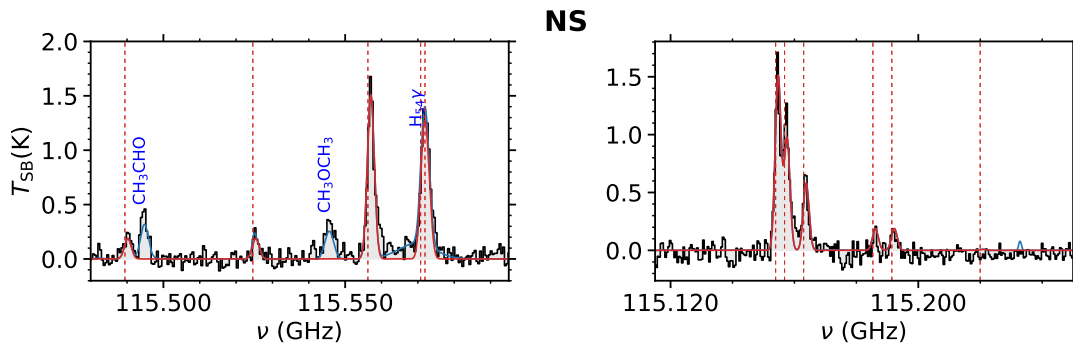


Fig. S 21: Transitions of NS detected toward the G31.41 shock position. The black histogram and its gray shadow are the observed spectrum. The red curve is the best LTE fit of the individual species and the blue curve is the cumulative fit considering all detected species. The red dashed lines indicate the frequency of the transitions that we are fitting. The plots are sorted by decreasing line intensity of the transitions.

## $C_2H_5OH$

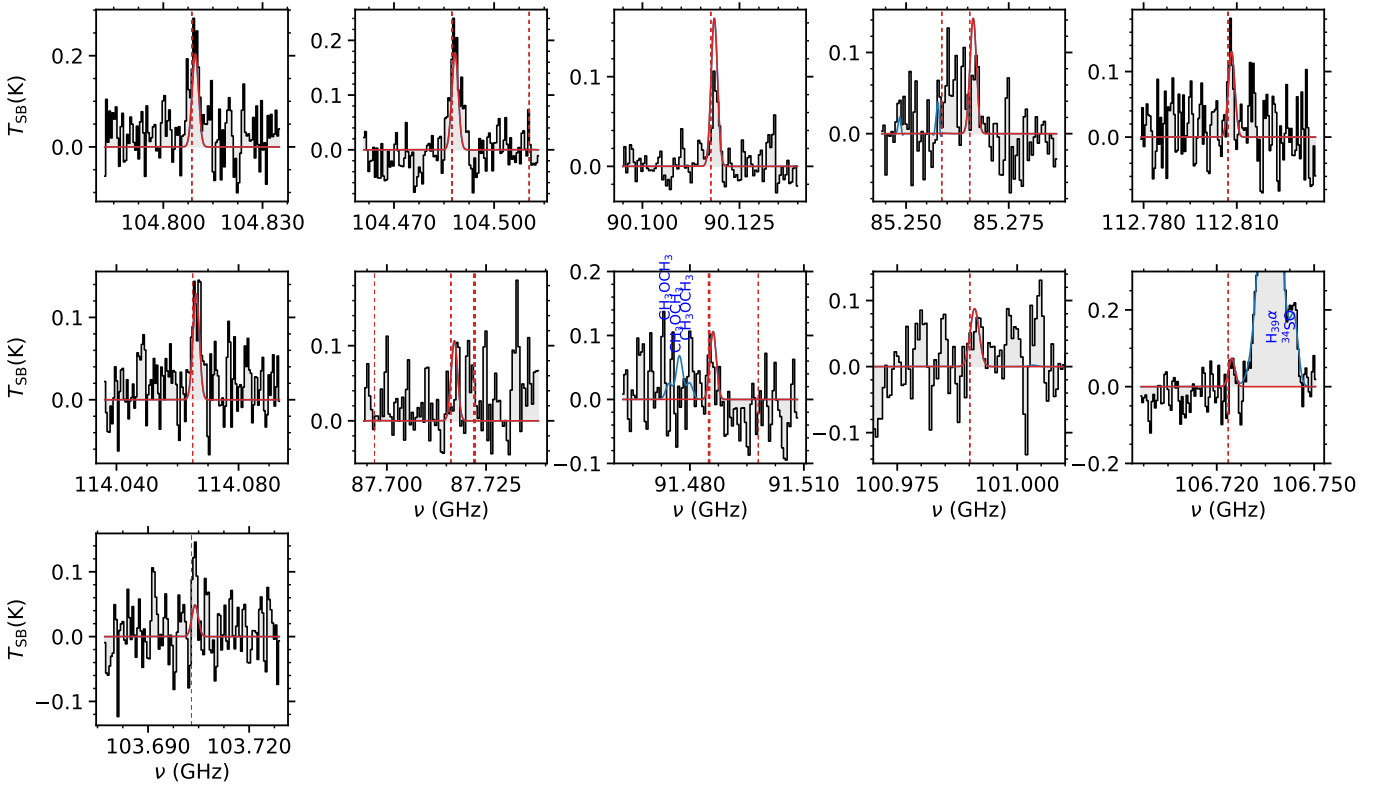


Fig. S 22: Transitions of  $C_2H_5OH$  detected toward the G31.41 shock position. The black histogram and its gray shadow are the observed spectrum. The red curve is the best LTE fit of the individual species and the blue curve is the cumulative fit considering all detected species. The red dashed lines indicate the frequency of the transitions that we are fitting. The plots are sorted by decreasing line intensity of the transitions.

### S 7. Spectra of additional detected molecules toward G31.41 core

We show here the spectra of the detected molecules toward the G31.41 core analyzed in this work. The results of the parameters obtained from the fits are summarized in Table B.3, and the information about the transitions used is listed in Table S 1.

### S 8. Spectra of additional not detected molecules toward G31.41 core

The spectra of the transitions used to obtain the column density upper limits toward the G31.41 core, presented in Table B.3, are shown in Fig. S 35, and the information about the transitions used is included in Table S 1. The upper limits are calculated by using the brightest transitions according to the LTE model that are not heavily blended, and by performing a visual inspection to make the upper limits compatible with the observed spectra (explained in more detail in Sect. 3.2.2).

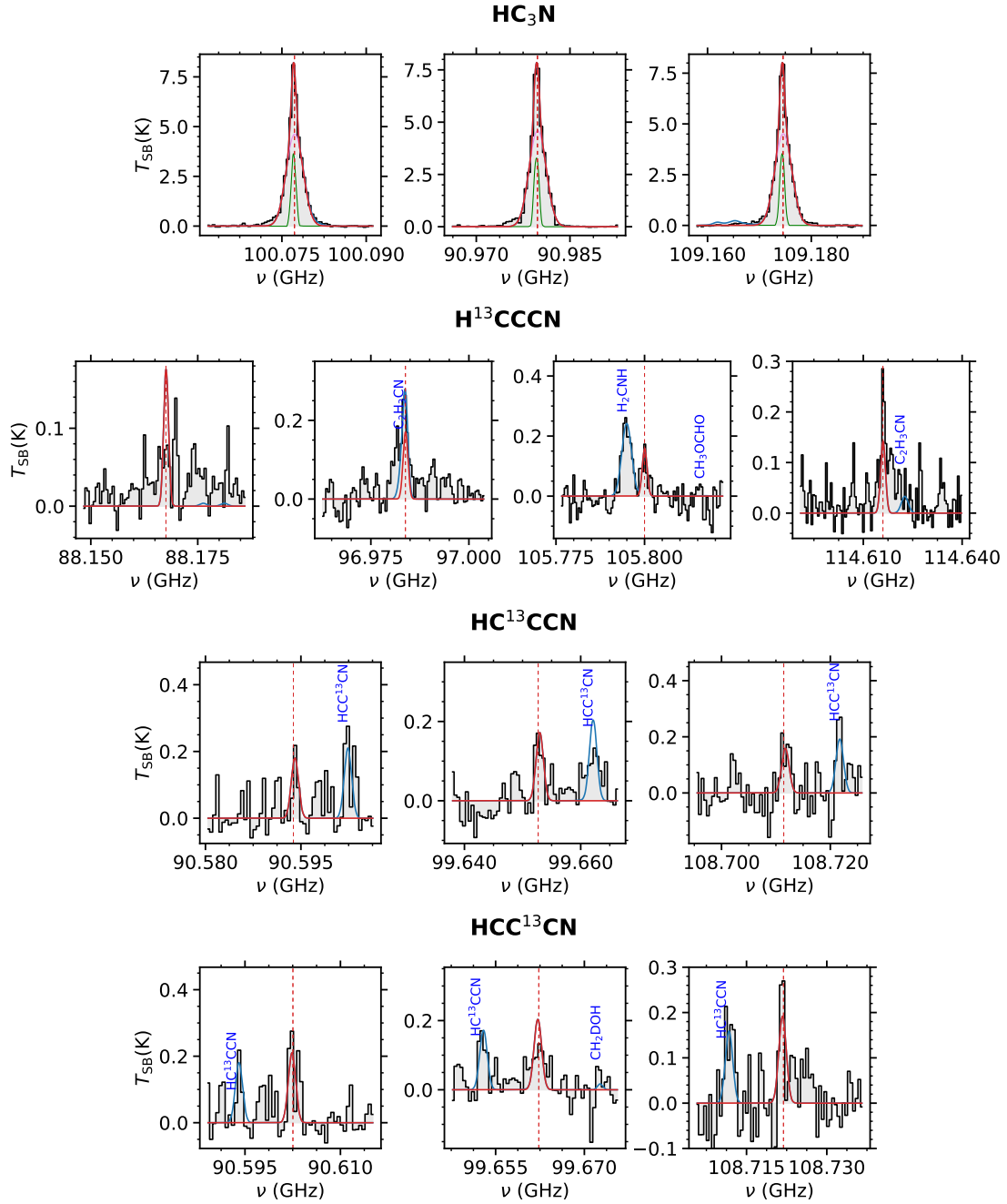


Fig. S 23: Transitions of HC<sub>3</sub>N isotopologs detected toward the G31.41 shock position. The black histogram and its gray shadow are the observed spectrum. The red curve is the best LTE fit of the individual species and the blue curve is the cumulative fit considering all detected species. The red dashed lines indicate the frequency of the transitions that we are fitting. The plots are sorted by decreasing line intensity of the transitions. For HC<sub>3</sub>N, we used two components to fit, plotted in pink and green. In these cases, the red curve is the sum of both components.

### $C_2H_3CN$

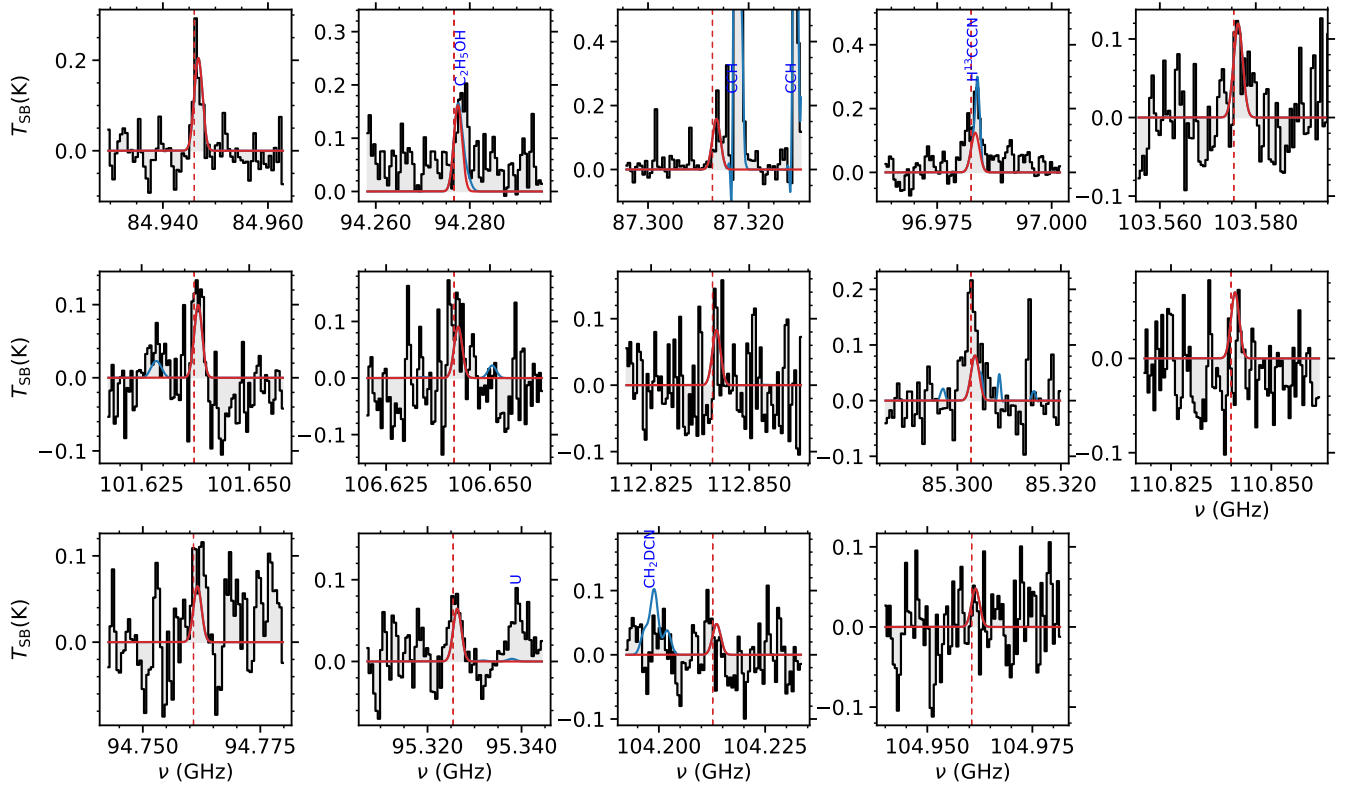


Fig. S 24: Transitions of  $C_2H_3CN$  detected toward the G31.41 shock position. The black histogram and its gray shadow are the observed spectrum. The red curve is the best LTE fit of the individual species and the blue curve is the cumulative fit considering all detected species. The red dashed lines indicate the frequency of the transitions that we are fitting. The plots are sorted by decreasing line intensity of the transitions. The label U in the plots indicates that the emission corresponds to an unidentified species.

### $CH_3OCHO$

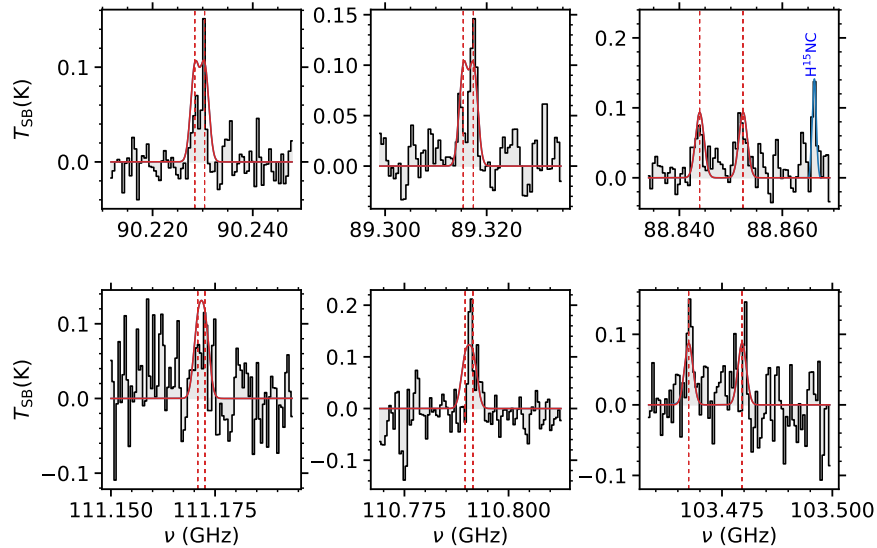


Fig. S 25: Transitions of  $CH_3OCHO$  detected toward the G31.41 shock position. The black histogram and its gray shadow are the observed spectrum. The red curve is the best LTE fit of the individual species and the blue curve is the cumulative fit considering all detected species. The red dashed lines indicate the frequency of the transitions that we are fitting. The plots are sorted by decreasing line intensity of the transitions.

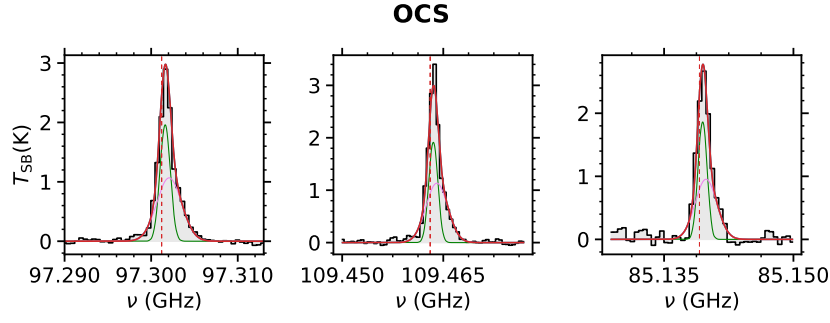


Fig. S 26: Transitions of OCS detected toward the G31.41 shock position. The black histogram and its gray shadow are the observed spectrum. There are two components fitted (the pink and green curves) which are the best LTE fit of the individual species, the red curve is the sum of the two components and the blue curve is the cumulative fit considering all detected species. The red dashed lines indicate the frequency of the transitions that we are fitting. The plots are sorted by decreasing line intensity of the transitions.

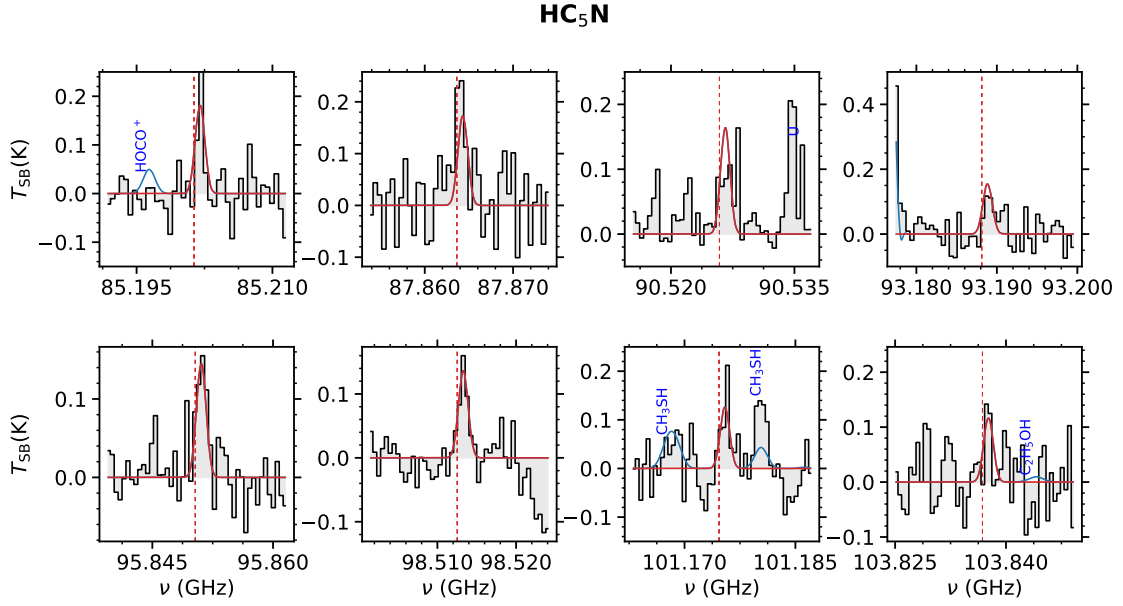


Fig. S 27: Transitions of HC<sub>5</sub>N detected toward the G31.41 shock position. The black histogram and its gray shadow are the observed spectrum. The red curve is the best LTE fit of the individual species and the blue curve is the cumulative fit considering all detected species. The red dashed lines indicate the frequency of the transitions that we are fitting. The plots are sorted by decreasing line intensity of the transitions. The label U in the plots indicates that the emission corresponds to an unidentified species.



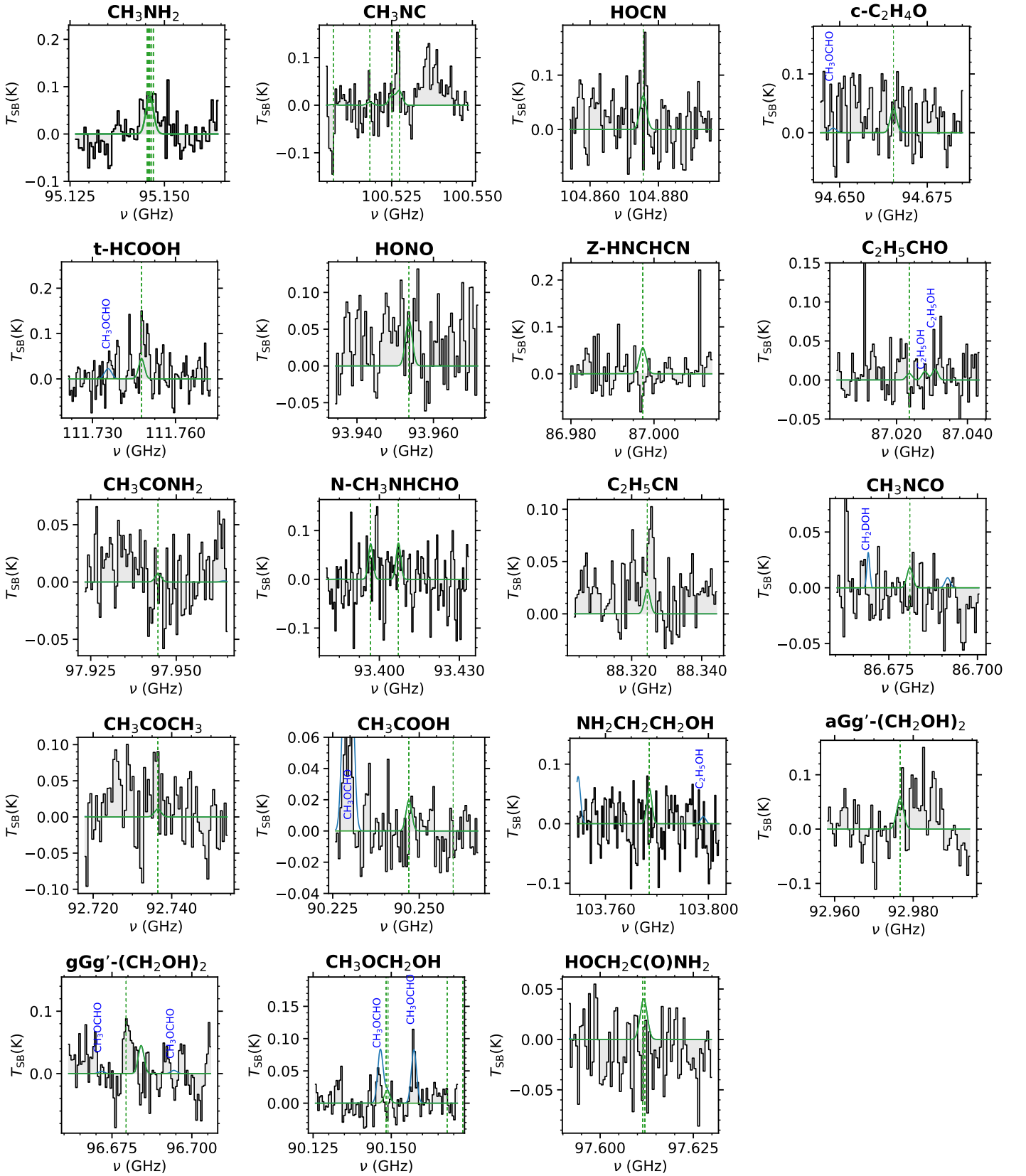


Fig. S 28: Molecules not detected toward the G31.41 shock position. The black histogram and its gray shadow are the observed spectrum. The LTE synthetic spectra using the derived upper limits of  $N$  are indicated with green curves. To compute the upper limits of their molecular abundances we have used the brightest and less blended transitions of each molecule, which are shown here. The green dashed lines indicate the frequency of the molecular transitions.

**NH<sub>2</sub>D**

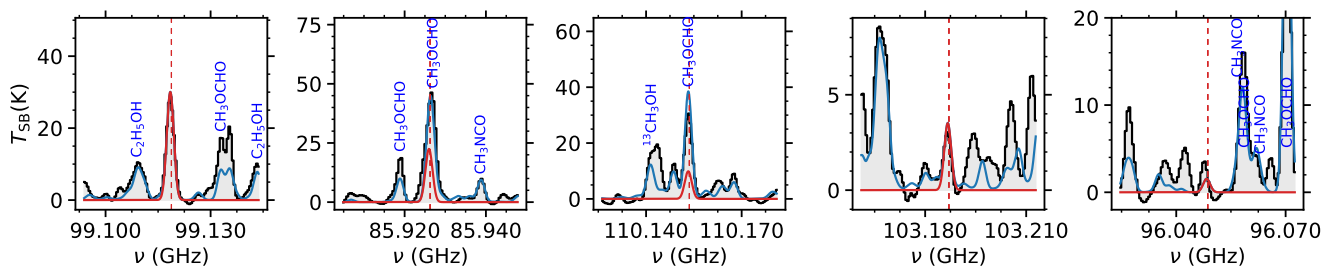


Fig. S 29: Transitions of  $\text{NH}_2\text{D}$  detected toward the G31.41 core position. The black histogram and its gray shadow are the observed spectrum. The red curve is the best LTE fit of the individual species and the blue curve is the cumulative fit considering all detected species. The red dashed lines indicate the frequency of the transitions that we are fitting. The plots are sorted by decreasing line intensity of the transitions.

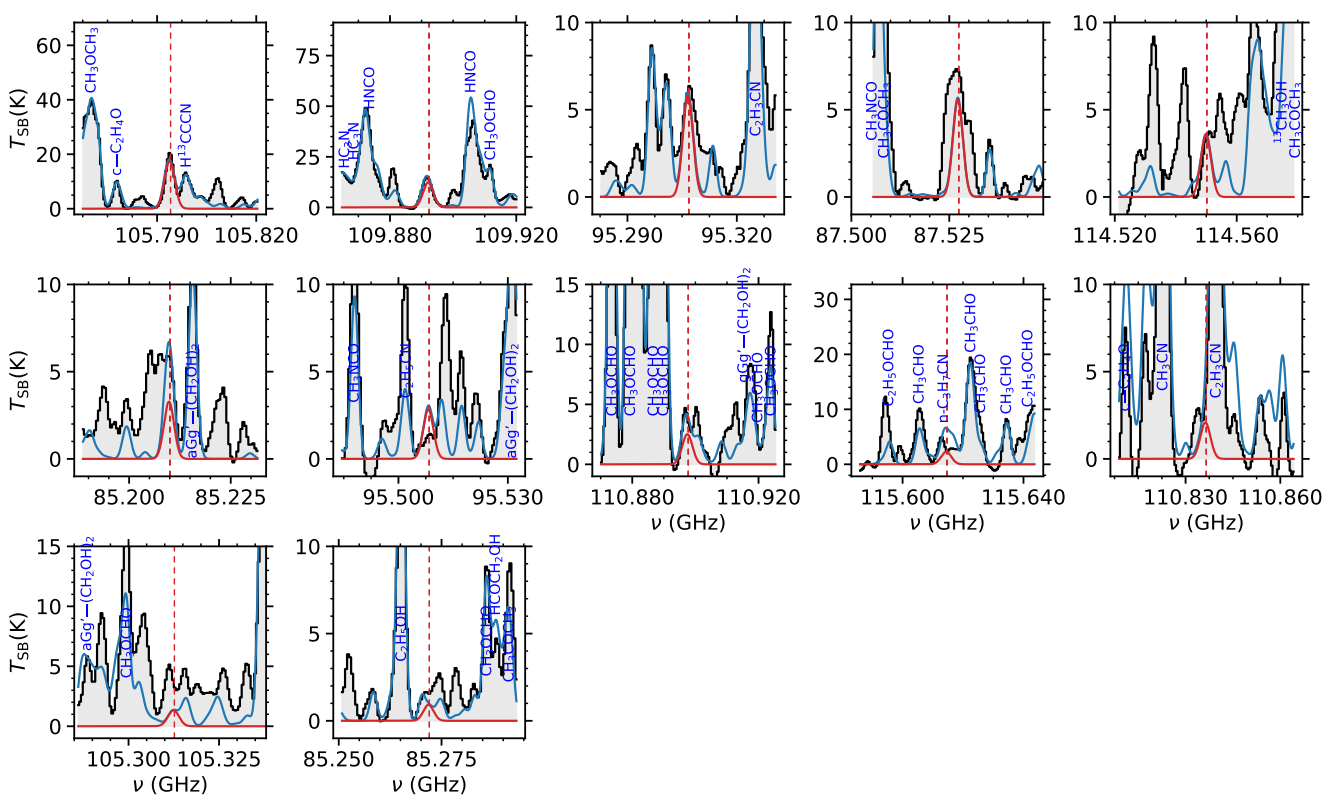
$$\mathbf{H_2CNH}$$


Fig. S 30: Transitions of  $\text{H}_2\text{CNH}$  detected toward the G31.41 core position. The black histogram and its gray shadow are the observed spectrum. The red curve is the best LTE fit of the individual species and the blue curve is the cumulative fit considering all detected species. The red dashed lines indicate the frequency of the transitions that we are fitting. The plots are sorted by decreasing line intensity of the transitions.

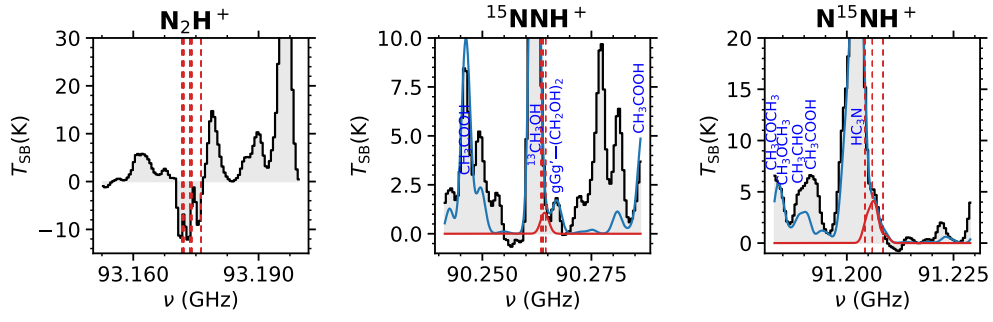
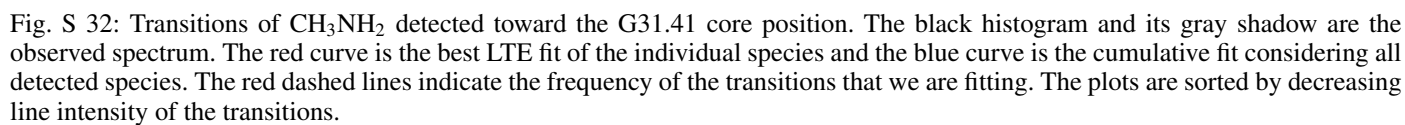


Fig. S 31: Transitions of  $\text{N}_2\text{H}^+$  isotopologs detected toward the G31.41 core position. The black histogram and its gray shadow are the observed spectrum. The red curve is the best LTE fit of the individual species and the blue curve is the cumulative fit considering all detected species. The red dashed lines indicate the frequency of the transitions that we are fitting. The plots are sorted by decreasing line intensity of the transitions.



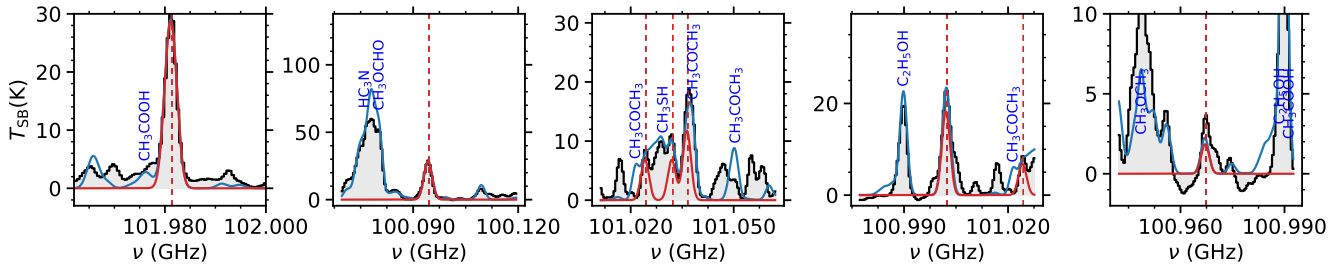
$$\text{H}_2\text{CCO}$$


Fig. S 33: Transitions of  $\text{H}_2\text{CCO}$  detected toward the G31.41 core position. The black histogram and its gray shadow are the observed spectrum. The red curve is the best LTE fit of the individual species and the blue curve is the cumulative fit considering all detected species. The red dashed lines indicate the frequency of the transitions that we are fitting. The plots are sorted by decreasing line intensity of the transitions.

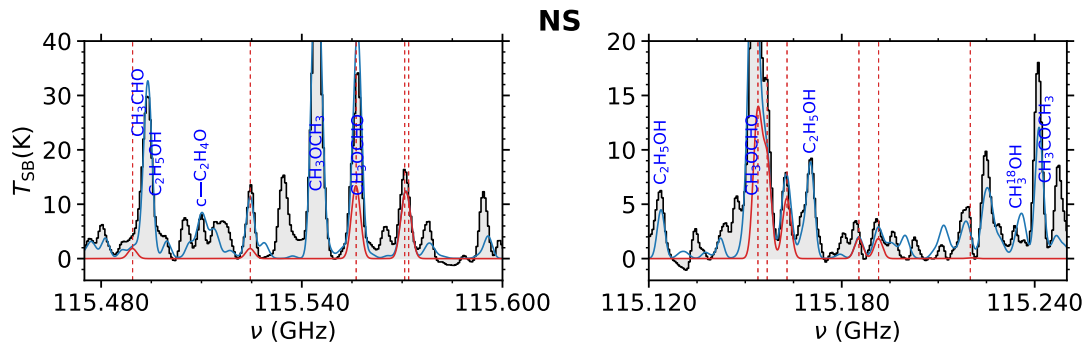


Fig. S 34: Transitions of NS detected toward the G31.41 core position. The black histogram and its gray shadow are the observed spectrum. The red curve is the best LTE fit of the individual species and the blue curve is the cumulative fit considering all detected species. The red dashed lines indicate the frequency of the transitions that we are fitting. The plots are sorted by decreasing line intensity of the transitions.

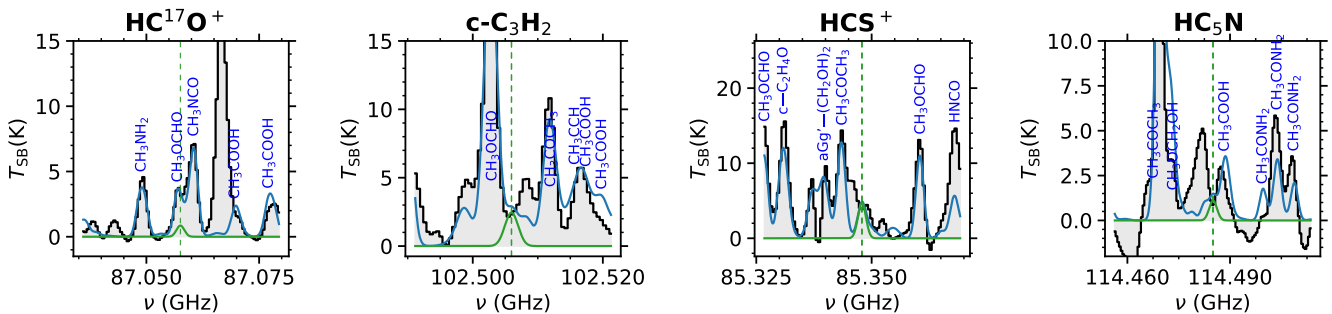


Fig. S 35: Additional molecules not detected toward the G31.41 core position. The black histogram and its gray shadow are the observed spectrum. The LTE synthetic spectra using the derived upper limits of  $N$  are indicated with green curves. To compute the upper limits of their molecular abundances we have used the brightest and less blended transitions of each molecule, which are shown here. The green dashed lines indicate the frequency of the molecular transitions.

## References

Suzuki, T., Majumdar, L., Goldsmith, P. F., et al. 2023, ApJ, 954, 189